ABSTRACT

CABRAL, MATTHEW JOHN. Electrical Characterization of Radiation Induced Defects in 3C-SiC. (Under the direction of Steven C. Shannon).

Silicon carbide is an important material which has application in both state of the art circuitry and in extreme environment MEMS applications. Due to its excellent high temperature mechanical properties, 3C silicon carbide is being considered as a coating material for generation IV reactor TRISO fuel particles. The 3C-SiC will serve to contain fission byproducts emitted by nuclear fuel. Given the application, it is important to understand and characterize the evolution of radiation damage in the 3C-SiC lattice. In this work, electrical characterization will be used as a means of detecting and quantifying radiation damage in 3C-SiC thin films.

The 3C-SiC investigated is polycrystalline in structure and is grown on silicon substrates via a LPCVD at 900°C using dicholorsilane and acetylene as the precursors. The 3C-SiC films were also in-situ doped during the film growth by adding ammonia as a source of n-type nitrogen dopants. Utilizing the 3C-SiC thin films; a p-n junction structure was formed by depositing n-type 3C-SiC on a p-type silicon substrate and sheet resistance samples were formed by electronically isolating the 3C-SiC from the silicon substrates with a layer of silicon dioxide. Current-voltage characteristics and resistivity measurements were taken for a series of samples. These samples were then irradiated with 1 MeV Si^+ ions for ion flux values between $5x10^{12}$ ions/cm^2 and $1x10^{15}$ ions/cm^2 using an ion beam at UT Knoxville. The post irradiation electrical data yielded several important results.

The slope of the I-V curves resulting from the p-n junctions, tended to broaden as ion fluence was increased. Slope broadening was evident at very small ion flux values, which correspond to a dpa of approximately ~0.001. For resistivity, eight samples irradiated at different ion fluence values demonstrated a gradual increase in resistivity until the ion flux increased from 10^{14} ions/cm^2 to $5x10^{14}$ ions/cm^2. At this point the increase in resistivity was significant. The trend demonstrated by the resistivity indicates the evolution of radiation damage in the 3C-SiC films. Small ion fluences (dpa of ~0.001) create point defects in the film which recombine at the grain boundaries. At larger fluences (dpa of ~0.1), as confirmed with TEM imaging, the film begins to transition from crystalline to crystalline/amorphous.

The results obtained in this work indicate that electrical characterization is an effective means of detecting low levels of radiation damage in 3C-SiC. Additionally the evolution of defects in the crystal structure can be related to electrical response.

.

© Copyright 2013 by Matthew J. Cabral

All Rights Reserved

Electrical Characterization of Radiation Induced Defects in 3C-SiC

by
Matthew J. Cabral

A thesis submitted to the Graduate faculty of
North Carolina State University
in partial fulfillment of the
requirements for the Degree of
Master of Science

Nuclear Engineering

Raleigh, North Carolina

2013

APPROVED BY:

_______________________________ Dr. Mohamed A. Bourham

_______________________________ Dr. Jon-Paul Maria

_______________________________ Dr. Steven C. Shannon
Committee Chair

DEDICATION

To my Parents.

BIOGRAPHY

Matthew J. Cabral was born in Fall River, MA on June 28th 1988 to Manuel and Ana Cabral. He is the first of two sons and has a younger brother named Damien. After graduating from Bishop Stang High School in 2006, he attended Roger Williams University in Bristol, RI where he majored in engineering. In May 2010, he received a Bachelor of Science Degree in Mechanical Engineering. Soon after graduation he moved to Raleigh, NC where he began his graduate career in the Department of Nuclear Engineering at North Carolina State University. In the fall of 2010 he began working under the direction of Dr. Steven Shannon.

ACKNOWLEDGEMENTS

I would like to begin by thanking Dr. Steven Shannon for all he has done for me the last few years. Not just for giving me a chance to work for him, but for all the guidance and support he has provided me since beginning at NC State. I don't think I could have made it without him, so I would like to sincerely thank him for everything. I would also like to thank the members of my committee, Dr. Mohamed Bourham and Dr. JP Maria for making the time to review this work. I greatly appreciate both your time.

I want to express my thanks to the NNF staff for all the assistance that they have provided me throughout my time in the cleanroom. It would not have been possible to complete this project without them. I would also like to thank Yanwen Zhang and Bill Weber along with their graduate students at the University of Tennessee for helping conduct the experiments discussed in this report. I would also like to thank Chris Hardiman for help he has provided me in completing this project. The cleanroom work would not have been as enjoyable without him around.

Finally, I would like to thank my parents, brother, and grandmother for their love and support that they have always provided me.

Funding for this project was provided by the Department of Energy Nuclear Energy University Partnership grant number 10-817.

TABLE OF CONTENTS

LIST OF TABLES vii

LIST OF FIGURES viii

Chapter 1: Introduction to SiC and its Applications 1

1.1 Motivation 1
1.2 Fuel Particle Coatings 3
1.3 Fuel Cladding 4
1.4 Structure and Mechanical Properties of SiC 5
1.5 Electrical Properties of SiC 7
1.6 Thesis Overview 10

Chapter 2: Device and Sample Fabrication 11

2.1 Substrate Preparation 11
2.2 Material Synthesis and Doping via CVD 12
2.3 TEM Imaging of 3C-SiC 21
2.4 Resistivity Samples 24
2.5 Fabrication of p-n Junction Diodes 28

Chapter 3: Device Irradiation 43

3.1 Ion Beam System 43
3.2 Sample Mounting and Irradiation Conditions 45
3.3 Irradiation Simulations using TRIM Software 48

Chapter 4: Characterization Methods 59

4.1 Keithley® 4200 SCS and Four Point Probe 59
4.2 Resistivity Measurements 63
4.3 Current-Voltage (IV) Curves 65

Chapter 5: Results and Analysis 68

5.1 Resistivity vs. Fluence 68
5.2 Resistivity vs. Fluence Analysis and Discussion 72
5.3 I-V Curves..78
5.4 I-V Curve Analysis and Discussion..80

Chapter 6: Conclusions and Future Work..85

6.1 Conclusions..85
6.2 Future Work 87

REFERENCES 89

APPENDICES.. 94

Appendix A..95

LIST OF TABLES

Table 2.1: Thickness of SiO_2 Layers on Five Silicon Wafers after Oxidation 27

Table 2.2: Process Conditions used for p-n Junction and Resistivity Samples 35

Table 2.3: Resistivities, Mobility, Acceptor Concentration, and Donor Concentration for Si and 3C-SiC 37

Table 2.4: p-n Junction Parameters...39

Table 3.1: Target Fluences for Resistivity Samples 47

Table 3.2 Target Fluences for p-n Junction Samples...47

Table 4.1: Preirradiation Sheet Resistance/Sample Resistivity Measurements for a 178.5 nm 3C-SiC Film 64

Table 4.2: Preirradiation Sheet Resistance/Sample Resistivity Measurements for a 328.5 nm 3C-SiC Film 65

Table 5.1 Initial and Final Resistivity Values for each 178.5 nm 3C-SiC Sample.................68

Table 5.2: Initial and Final Resistivity Values for each 328.5 nm 3C-SiC Sample 70

Table 5.3: DPA Values 178.5 nm Thick 3C-SiC Resistivity Samples 73

Table 5.4: DPA Values 328.5 nm Thick 3C-SiC Resistivity Samples 74

Table 5.5: DPA Values for Al/SiC/Si/Au Structures with 178.5 nm and 328.5 nm of 3C-SiC 81

Table 5.6: Increase in Resistance and Resistivity Comparison for Al/SiC/Si/Au and Electronically Isolated 3C-SiC Samples with a Film Thickness of 178.5 nm 82

Table 5.7: Increase in Resistance and Resistivity Comparison for Al/SiC/Si/Au and Electronically Isolated 3C-SiC Samples with a Film Thickness of 328.5 nm 82

LIST OF FIGURES

Figure 1.1: TRISO Fuel Particle 3

Figure 1.2: Structure of Several Silicon Carbide Polytypes 6

Figure 1.3: Forward Bias IV Characteristics for a 4H-SiC Schottky Diode, Pre and Post Irradiation with 24 GeV/c Protons 9

Figure 2.1: Typical LVCVD Furnace Illustration 13

Figure 2.2: Deposition Rate as a Function of Pressure at 900°C 16

Figure 2.3: Residual Stress of 3C-SiC Films as a Function of Pressure 17

Figure 2.4: Visual Representation of the LPCVD Process used to Grow Poly 3C-SiC 19

Figure 2.5: TEM Image of a Tensile 3C-SiC Thin Film at 40,000x 22

Figure 2.6: TEM Image of a Compressive 3C-SiC Thin Film at 40,000x 23

Figure 2.7: Oxide Thickness vs. Time at 950°C for the NCSU NNF Dry Oxidation Process 26

Figure 2.8: Illustration of Sample used for Resistivity Measurements 28

Figure 2.9: Flowchart Outlining the Procedure used to Fabricate Resistivity and p-n Junction Samples 31

Figure 2.10: Resistive Heating Evaporator Located in the NCSU Cleanroom 40

Figure 2.11: DC Sputtering used to Deposit Gold Contacts 41

Figure 2.12: Cross Section of the p-n Junction Structure 42

Figure 3.1: Ion Beam System at the University of Tennessee in Knoxville 44

Figure 3.2: Vacuum Chamber which Housed the Samples to be Irradiated 45

Figure 3.3: Stainless Steel Slat that Samples were Mounted on 46

Figure 3.4: Depth vs. Y-axis for SiC(178.5 nm)/SiO_2/Si Structure 49

Figure 3.5: Depth vs. Y-axis for SiC(328.5 nm)/SiO_2/Si Structures 49

Figure 3.6: Ion Ranges for 1 MeV Ions into SiC(178.5 nm)/SiO_2/Si 50

Figure 3.7: Ion Ranges for 1 MeV Ions into SiC(328.5 nm)/SiO_2/Si 51

Figure 3.8: Collision Events for 1 MeV Ions into SiC(178.5 nm)/SiO_2/Si.............................52

Figure 3.9: Collision Events for 1 MeV Ions into SiC(328.5 nm)/SiO_2/Si.............................53

Figure 3.10: Depth vs. Y-axis for Al/SiC(178.5 nm)/Si Structure 54

Figure 3.11: Depth vs. Y-axis for Al/SiC(328.5 nm)/Si Structure 54

Figure 3.12: Ion Ranges for Al/SiC(178.5 nm)/Si Structure 55

Figure 3.13 Ion Ranges for Al/SiC(328.5 nm)/Si Structure 56

Figure 3.14: Collision Events for Al/SiC(178.5 nm)/Si Structure..57

Figure 3.15: Collision Events for Al/SiC(328.5 nm)/Si Structure..58

Figure 4.1: Keithley® 4200 SCS used to Characterize p-n Junctions....................................59

Figure 4.2: Four-Point Probe used for Resistivity Measurements of 3C-SiC..........................61

Figure 4.3: Collinear Four Point Probe Illustration 62

Figure 4.4: I-V Curve for Al/SiC/Si/Au Structure with 178.5 nm of 3C-SiC 66

Figure 4.5: I-V Curve for Al/SiC/Si/Au Structure with 328.5 nm of 3C-SiC 67

Figure 5.1: Increase in Resistivity vs. Ion Fluence for 178.5 nm 3C-SiC films 69

Figure 5.2: Increase in Resistivity vs. Ion Fluence for 328.5 nm 3C-SiC Films 71

Figure 5.3: Unirradiated Films (a&d) Compared to Films
Irradiated at 0.09 dpa (b&e) 75

Figure 5.4: Unirradiated Films (a&d) Compared to Films
Irradiated at 0.49 dpa (c&f) 76

Figure 5.5: Pre and Post Irradiation I-V Curves for the
Al/SiC(178.5nm)/Si/Au Device 79

Figure 5.6: Pre and Post Irradiation I-V Curves for the
Al/SiC(328.5nm)/Si/Au Device 80

Chapter 1

Introduction to SiC and its Applications

1.1 Motivation

With the current fleet of nuclear power plants in the United States aging and the development of new reactors occurring worldwide, several materials are being investigated for employment in the next generation of nuclear reactors. Currently functioning reactors have a lifetime of approximately 40 years, with the option of having the license extended by an additional 20 years if the reactor passes inspection. Given the high cost of building and maintaining a reactor, engineers aim to extend the minimum and maximum lifetime of next generation reactors in order to optimize the profitability of building and operating nuclear reactors without sacrificing safety. With this challenge comes the need to develop reactor components which will last the lifetime of the reactor, from first power up to final decommissioning. Additionally, the aim for improved reactor safety is a major consideration in the research for materials which will be able to tolerate the high temperatures and radiation levels in the extreme environment of a nuclear reactor.

A current topic of interest in the nuclear industry is the design of next generation reactor fuel. There are many proposed generation IV reactor designs, but most of these reactors would utilize similar fuel. One of the most researched fuel designs is known as TRISO fuel. This fuel can best be described as tiny uranium dioxide particles coated with

several layers of structural material [40]. Cubic Silicon carbide (3C-SiC) is among the layers coating the uranium dioxide particles. 3C-SiC plays an important role as a fuel particle coating; it serves to contain fission byproducts emitted by the fuel. Given the application, many researchers are investigating the accumulation of radiation damage in 3C-SiC.

There are many methods used to characterize radiation damage in silicon carbide. Commonly used methods include simulations, the use of analytical instrumentation, and electrical characterization. Analytical instrumentation such as transmission electron microscopes (TEM) and x-ray diffraction (XRD) are effective at characterizing large scale material defects, but may become less effective at low levels of radiation accumulation. Electrical testing will provide a more effective means of characterizing low levels of radiation damage accumulation in 3C-SiC. The bandgap of 3C-SiC is 2.4 eV, classifying it as a semiconductor. Given its electrical properties, it is possible to fabricate electrical devices such as p-n junctions with 3C-SiC. The electrical response of the 3C-SiC devices to radiation damage can then be used as a means of quantifying various levels of radiation damage, particularly at low levels.

The objective of this work is to fabricate and employ 3C-SiC devices as a means of measuring radiation damage accumulation from electrical response of the devices. The silicon carbide which is the subject of this investigation is polycrystalline n-type 3C-SiC. This material is grown on silicon substrates via low pressure chemical vapor deposition (LPCVD). Devices including p-n junctions and sheet resistance samples are fabricated and electrically characterized before and after irradiation. These experiments will provide an

understanding of how electrical properties change with radiation damage. These changes in electrical properties are then related to the evolution of defects occurring in the 3C-SiC.

1.2 Fuel Particle Coatings

There are numerous candidate materials currently being considered for implementation in the next generation of nuclear reactors. One application 3C-SiC is currently being considered for is as a fuel particle coating. These particles are known as TRISO fuel, and a diagram of one of these particles can be seen below in Figure 1 [24].

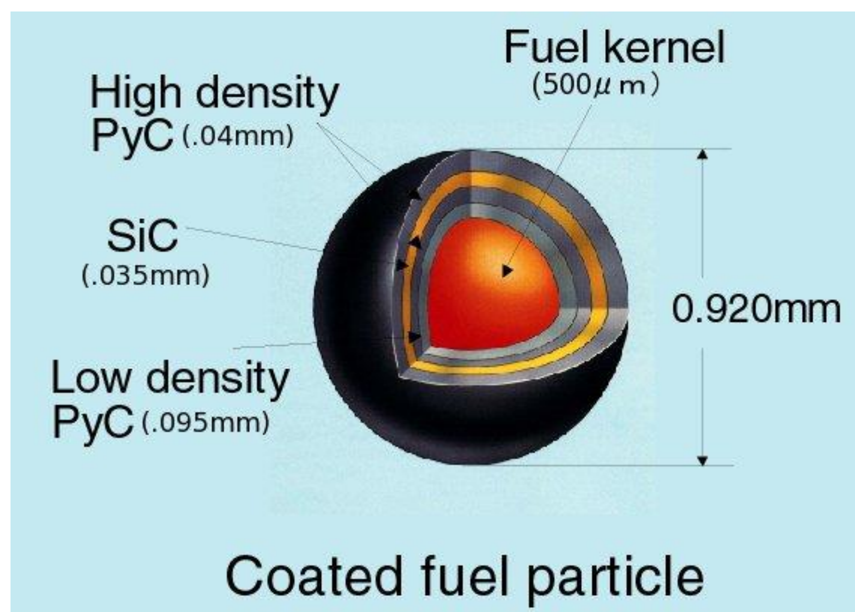

Figure 1.1: TRISO Fuel Particle

Many reactor designs proposed for the next generation fleet utilize TRISO fuel particles. This fuel form consists of small particles (on the order of 1000 microns) that are spheres of fissile

material coated with pyrolytic carbon and 3C-SiC [37]. The silicon carbide layer serves several purposes, but is mainly used for maintaining structural integrity of the fuel.

The TRISO fuel structure applies as a variety of generation IV rector designs. An example of a generation IV nuclear reactor which would employ TRISO fuel would be the very high temperature gas cooled reactors. There are several configurations for the reactor core which could be of either a prismatic block or pebble bed design [36]. Prismatic blocks are tiny cylindrical pellets (49.3 mm in length by 12.45 mm in diameter) comprised of TRISO fuel particles surrounded by a graphite matrix. These pellets are then loaded into fuel rods which power the reactor [42]. Pebble bed reactor cores employ the TRISO fuel particles in a similar manner to the prismatic block cores. Rather than pellet design, pebble bed reactor fuel is comprised of 60 mm diameter pellets comprised of TRISO fuel particles in a graphite matrix. The core of the reactor is then loaded with approximately 360,000 of these pellets which powers the reactor [21, 23]. Given the harsh environment, the materials being used to coat the tiny fuel kernels must be able to maintain structural integrity in the presence of high temperatures and radiation [38, 45]. Silicon carbide has been chosen as the fuel kernel coating since it can withstand the reactor environment.

1.3 Fuel Cladding

Fuel cladding is an important part of a nuclear reactor. Cladding serves several objectives but its main purpose is to separate the nuclear fuel from the surrounding coolant and serve as primary containment in the event of an accident. If cladding material were to

fail, then there would be a possibility that radioactive material would leak into the coolant, and subsequently into the environment. Overall, nuclear fuel cladding must: have a small neutron absorption cross section, be thermally conductive, and have a small coefficient of thermal expansion. These requirements must be kept for the lifetime of the fuel in the reactor. A common problem with occurs in fuel cladding is embrittlement and swelling due to nuclear reactions within the cladding material [3]. Based on current research, 3C-SiC is an excellent candidate material for fuel cladding since it has favorable high temperature properties, high mechanical strength, and radiation tolerant properties.

In order for 3C-SiC to replace current cladding materials, it must have a higher degree of radiation tolerance and strength at high levels of radiation. The current generation of reactors currently employ alloys comprised of zirconium known as zircaloys as cladding materials. In addition to zirconium, other materials which comprise the alloy include tin, niobium, iron, chromium, and nickel. Zircaloys are excellent cladding materials since they have a low neutron absorption cross section, high hardness, and are corrosion resistant [49]. 3C-SiC shares many of these properties, but further testing on the accumulation of radiation damage in the 3C-SiC is necessary.

1.4 Structure and Mechanical Properties of SiC

Silicon carbide is a semiconducting material which has improved mechanical properties when compared to silicon. There are over 200 different polytypes of SiC, where each polytype differs in the arrangement of the silicon and carbon atoms relative to each

other. The most commonly applied polytypes of silicon carbide include the 3C, 4H, and 6H structures. The C in 3C stands for a cubic structure, while the H in 4H and 6H stands for hexagonal. All polytypes are similar in 2 dimensions, but differ in the third dimension, which is the stacking form. An illustration of the structure of several SiC polytypes can be seen below in Figure 1.2 [8].

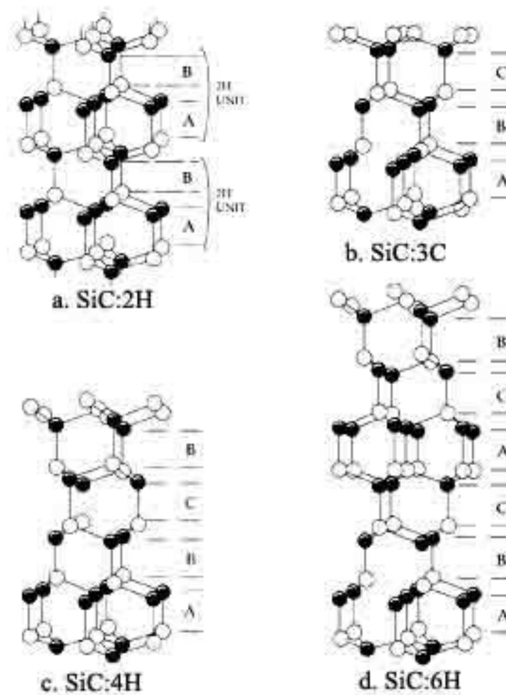

Figure 1.2: Structure of Several Silicon Carbide Polytypes

There are numerous benefits for application of the different polytypes of silicon carbide. The 4H and 6H polytypes demonstrate excellent properties for fabricating electrical devices for application in extreme environments. Studies performed on devices fabricated from 4H and 6H-SiC have produced electrical properties superior to those of silicon devices,

and benefit from a much higher melting point. The melting point of 4H-SiC is 2800°C; double the 1400°C melting point of silicon. The high melting points of 4H and 6H-SiC allow for their application in high temperature environments [6].

Numerous studies have already been performed on 3C-SiC to determine its mechanical properties. 3C-SiC is most commonly used for the fabrication of micro electromechanical systems (MEMS) due to its superior mechanical properties and because it can be deposited on silicon substrates unlike 4H and 6H-SiC [18]. The melting temperature of 3C-SiC is approximately 2700°C which is much larger than the 1400°C melting temperature of bare silicon. Additionally, the Young's Modulus has been determined to be approximately 394 GPa, while the thermal expansion coefficient is $4.2*10^{-6}$/°C. The hardness of 3C-SiC has also been observed to be 9.2 on the Mohs scale, which can be compared to diamond which has a Mohs value of 10 [44, 55]. The low thermal expansion coefficient will allow for structural integrity of the fuel under operating temperatures, which is an important factor when considering safety. Due to all these factors, 3C-SiC is a prime candidate for coating fourth generation reactor fuel.

1.5 Electrical Properties of SiC

The electrical properties of 3C-SiC have been observed to vary from the properties of the more commonly used 4H and 6H polytypes. The band gap of 3C-SiC is approximately 2.4 eV, which is smaller than the band gaps of 4H and 6H silicon carbide which ranges from 3 to 3.5 eV. In comparison, the band gap of common semiconductors such as silicon and

germanium are 1.12 eV and 0.67 eV respectively. The dielectric constant of all three silicon carbide polytypes is approximately 9.7; lower than the 11.9 dielectric constant of silicon. The mobility of electrons and holes in all the three silicon carbide polytypes vary with dopant concentration. At a donor concentration of $10^{16}/cm^3$ the mobility of electrons (in $cm^2/V*s$) is 800 for 3C-SiC, 800 along the c-axis of 4H-SiC, and 400 along the c-axis of 6H-SiC. The hole mobility of all three polytypes are much lower than their corresponding electron mobility values. An acceptor concentration of $10^{16}/cm^3$ yields hole mobility values (in $cm^2/V*s$) of 115 for 3C-SiC, 40 for 4H-SiC, and 90 for 6H-SiC [4, 12]. Silicon carbide, notably the 4H polytype, has become a popular material for high power device fabrication.

The 4H and 6H polytypes of silicon carbide have become popular in the industry of high power electronic fabrication. Current state of the art semiconducting devices including p-n junctions and MOSFETS [6] have been fabricated by companies such as CREE®. These devices are very expensive to produce; since the cost of fabricating 4H and 6H-SiC is high. An application of 4H-SiC to a field other than that of high power electronics would be in the creation of radiation detectors. In a study performed by Nava et al., 4H-SiC devices were used for the detection of electron and protons. In one experiment discussed in the article, shifts were observed in the I-V characteristics of a 4H-SiC Schottky diode due to proton irradiation. Figure 1.3 below illustrates the results of the study on proton irradiation in 4H-SiC Schottky diodes [33]. As observed from the plot, the characteristic current values decrease when the devices are irradiated. It may be possible to attribute similar shifts in electrical properties to radiation damage accumulation in devices fabricated with 3C-SiC.

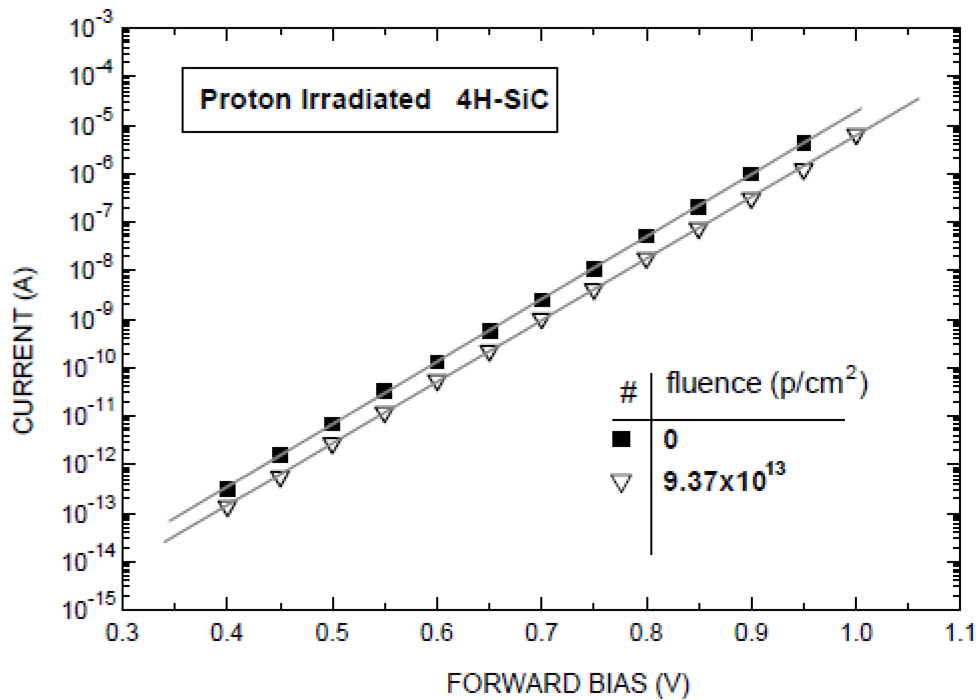

Figure 1.3: Forward Bias IV Characteristics for a 4H-SiC Schottky Diode, Pre and Post Irradiation with 24 GeV/c Protons

The 3C polytype is less commonly used in the electronics fabrication industry, but there have been several devices successfully fabricated with 3C-SiC. The highest quality 3C-SiC p-n junctions have been developed by NASA which consists of layers of single crystalline, doped 3C-SiC forming a junction between p-type and n-type layers grown on 6H silicon carbide substrates [34]. While high quality single crystalline 3C-SiC can be used to fabricate devices, the polycrystalline 3C-SiC investigated in this report is not an ideal candidate for device fabrication.

The application of any polycrystalline material for the production of electronic devices is not accepted in the fabrication industry. The crystal structure of polycrystalline

3C-SiC contains numerous microstructural defects including high densities of stacking faults, threading dislocations, and microtwins which result in poor electrical characteristics. Despite the down falls of producing electrical devices with polycrystalline 3C-SiC, information regarding the effects of radiation on these devices could prove to be valuable to determine the evolution of damage in the microstructure. It is important to note that the purpose of this study is not to fabricate an ideal 3C-SiC structure, but instead to leverage the useful albeit marginal electrical performance to elucidate radiation damage accumulation mechanisms in the 3C-SiC polytype which provides the greatest mechanical advantage for applications in extreme environments, specifically nuclear reactor systems.

1.6 Thesis Overview

The following chapters of this report will describe the fabrication, irradiation, and characterization of devices fabricated with 3C-SiC. Two types of devices were fabricated: p-n junctions and sheet resistance samples. The 3C-SiC films discussed were grown and in-situ doped using an LPCVD process. Once fabricated, the devices were electrically characterized using a Keithley® 4200 SCS and a four-point probe, before being irradiated. The irradiation experiments were performed using an ion beam located at the University of Tennessee in Knoxville. Following the irradiations, the samples were again electrically characterized. The pre and post irradiation results were then compared, and trends were drawn between the electrical characteristics and the accumulation of damage in the 3C-SiC.

Chapter 2

Device and Sample Fabrication

2.1 Substrate Preparation

The main advantage of using 3C-SiC for its various applications is the fact that it can be grown on silicon substrates unlike the 4H and 6H polytypes. It is also the preferential polytype for TRISO fuel forms due to its high temperature properties and radiation tolerance. The wafers used for the growth of polycrystalline 3C-SiC were commercially available, boron doped, 100 mm diameter <100> crystalline silicon substrates. The thickness of wafers ranged from 500 +/- 25 microns. The resistivity range of the wafers was between 0.001-0.005 Ω-cm. The low resistivity allows for the creation of p-n junctions with an appropriate depletion region in the 3C-SiC, which will be described in section 2.5. Additionally, the low resistivity of the wafers allow them to serve as a backside contact for a device on a probing station.

The wafers were thoroughly cleaned in order to remove any native oxides and contaminates from their surfaces. The cleaning of surface contaminates on the wafers was performed with a 10 minute RCA bath. Following the 10 minute bath, the wafers were rinsed six times with deionized water. Following the RCA clean, the wafers were then placed in a buffered oxide etch solution of diluted hydrofluoric acid for 2 minutes. The buffered oxide etch is performed in order to remove thin native oxide layers which could be detrimental to

electrical devices. Following the oxide etch, the wafers are again rinsed six times in deionized water and then placed in a spin dryer before being loaded into the LPCVD 3C-SiC furnace or the oxidation furnace. The process of 3C-SiC growth and oxidation are discussed in the proceeding sections.

2.2 Material Synthesis and Doping via LPCVD

There are numerous methods of synthesizing and depositing thin films on substrates. These are typically grouped into thermal passivation processes such as oxidation and nitridation, physical vapor deposition (PVD), and chemical vapor deposition (CVD). Other more exotic (and subsequently less utilized) deposition methods such as pulsed laser ablation deposition (PLAD), plasma enhanced chemical vapor deposition (PECVD), and ion beam assisted deposition (IBAD) are also employed for thin film deposition processes. Since these methods are not used in any of our fabrication processes, they are not discussed in detail in this report. Low pressure chemical vapor deposition (LPCVD) is used in order to deposit 3C-SiC thin films on silicon substrates for these experiments.

The main advantage of working with 3C-SiC as opposed to the 4H or 6H polytypes is the fact that thin films can be deposited on silicon substrates and that this deposition process can be run at lower temperatures then those required for other polytypes. Processing 4H and 6H silicon carbide is very expensive as it must be performed at very high temperatures (1400°C+). Temperatures this high are prohibitive for processes on substrates such as silicon with a melting temperature of 1400°C, or more practically, for processing in standard quartz

furnace tubes, where temperatures above 1100°C result in phase transitions in the quartz, subsequently generating particulate that can adversely impact the yield of devices fabricated. The 3C-SiC discussed in this work is grown at a much more reasonable temperature.

For the silicon carbide films studied here, the growth of polycrystalline 3C-SiC is performed at 900°C using a hot-wall, horizontal furnace as pictured below.

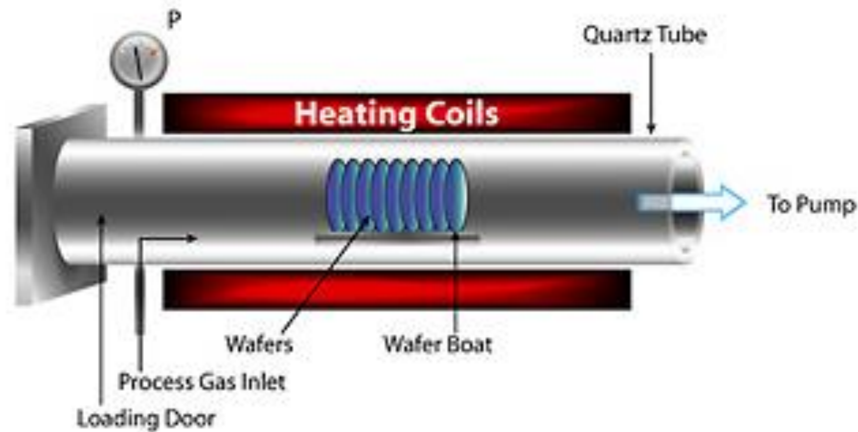

Figure 2.1: Typical LVCVD Furnace Illustration [2]

The wafers are contained in a quartz boat which once loaded, retracts into the furnace forming a vacuum seal. The furnace is heated via RF induction through a series of coils which encircle the quartz boat. Three thermocouples are located in the front, middle, and back of the furnace which allow for the monitoring of temperature throughout a deposition run. Additional components of the system include a vacuum system and a series of gas inlets which provide the feed gases required to deposit 3C-SiC.

Although the 3C-SiC formed via LPCVD is not a semiconductor grade material intended for the creation of devices, it demonstrates excellent radiation tolerant properties which make it a desirable material for future nuclear reactor applications. The radiation tolerant properties of the 3C-SiC grown using this LPCVD process have been the subject of an investigation by Zhang et al. A series of irradiations were performed on the 3C-SiC in order to determine the displacements per atom (dpa) required for complete amorphization of the film. The amorphization dose for the 3C-SiC is determined to be 3 dpa. In comparison, a dpa of 0.32 is required for the amorphization of single crystalline 3C-SiC [51]. The radiation tolerance of this polycrystalline 3C-SiC is the result of a high density of stacking faults within the individual grains of the silicon carbide. These stacking faults enhance the rate that which point defects recombine at the grain boundaries of the 3C-SiC. The results obtained by Zhang et al. will be discussed in comparison to the results of this study in subsequent chapters. The large number of stacking faults, created during film growth, is an inherent characteristic of this LPCVD process.

The process of chemical vapor deposition involves a chemical reaction of precursor gasses in a furnace [16]. In order for a reaction to occur, the change in free energy of the reaction needs to be negative. The change in free energy is a function of the furnace temperature as well as a function of stoichiometry of the gasses which are reacting. The change in free energy of the reaction can be described by:

$$\Delta G = -RT * \ln(K) \quad \text{Eq. 2.1}$$

Where R is the universal gas constant, *T* is the temperature, and *K* is the fraction of moles of the reactants and products. In order for a reaction to occur, the change in free energy must be negative. Since the films grown are polycrystalline, it can be assumed that the change in free energy is very negative resulting in a quicker nucleation rate. In order to form a single crystalline thin film, the reaction would need to occur at a slower rate. A larger temperature would allow for a larger grain size [13], but temperature is not a controllable furnace parameter, since the furnace is shared use. The temperature of 900°C is sufficient in order to break the bonds in the precursor gases of acetylene (C_2H_2) and dicholorsilane (SiH_2Cl_2, which will be referred to as DCS) which are the sources of the carbon and silicon atoms in 3C-SiC respectively [14, 15]. By performing numerous runs in the furnace, the effect of temperature and pressure on the polycrystalline 3C-SiC growth rate can be investigated.

The deposition rate of 3C-SiC on the silicon substrates is a function of both the furnace temperature and pressure. In both cases, the growth rate of 3C-SiC will increase as the temperature and/or pressure is increased [25]. A larger temperature results in a larger change in free energy causing a quicker nucleation rate, and thus faster growth rate. It must be noted that LPCVD furnace used for this experiment is a shared use tool, thus the temperature cannot be increased. Recalibration of thermocouples for temperature control can have adverse impact on baseline processes used by other users. Although it is possible to run the furnace at a lower temperature, decreasing the temperature would likely result in the growth of amorphous films [30]. This eliminates temperature as a variable for thin film parameter control. Since the temperature of the furnace cannot be changed, the pressure is

the only parameter which can be varied to change the growth rate. Figure 2.2 below illustrates the dependence of the silicon carbide growth rate on furnace pressure [17].

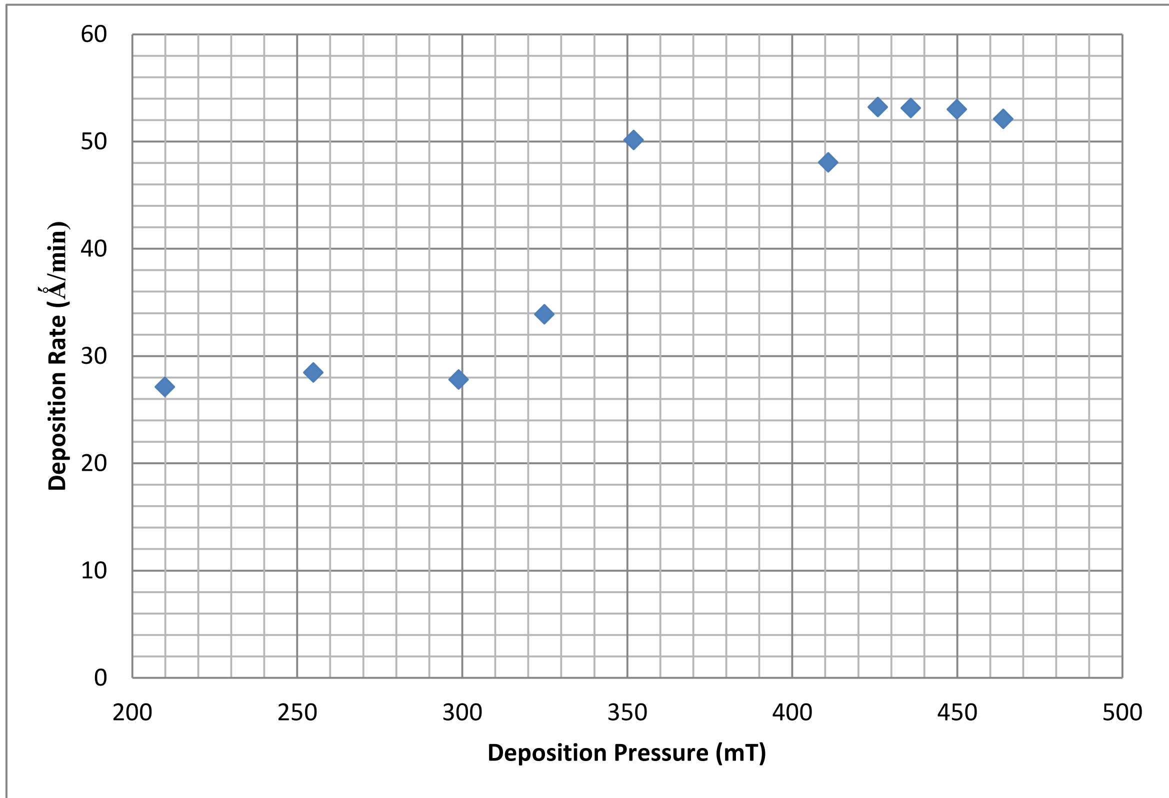

Figure 2.2: Deposition Rate as a Function of Pressure at 900°C

The data illustrated in Figure 2.2 above was obtained from a parametric study of deposition pressure on silicon carbide film characteristics for the NCSU furnace. In addition to affecting the growth rate of the film, the deposition pressure also has an effect on the residual film stress.

There is clear effect of deposition pressure on the residual stress of 3C-SiC films. Lower pressures result in tensile films while higher pressures result in compressive films. Stress testing is a commonly used metric for characterizing silicon carbide and is often the focus of 3C-SiC MEMS characterization [20] The stress dependence on pressure has been characterized for the NCSU 3C-SiC furnace using a wide range of growth pressures as illustrated below in Figure 2.3 [17].

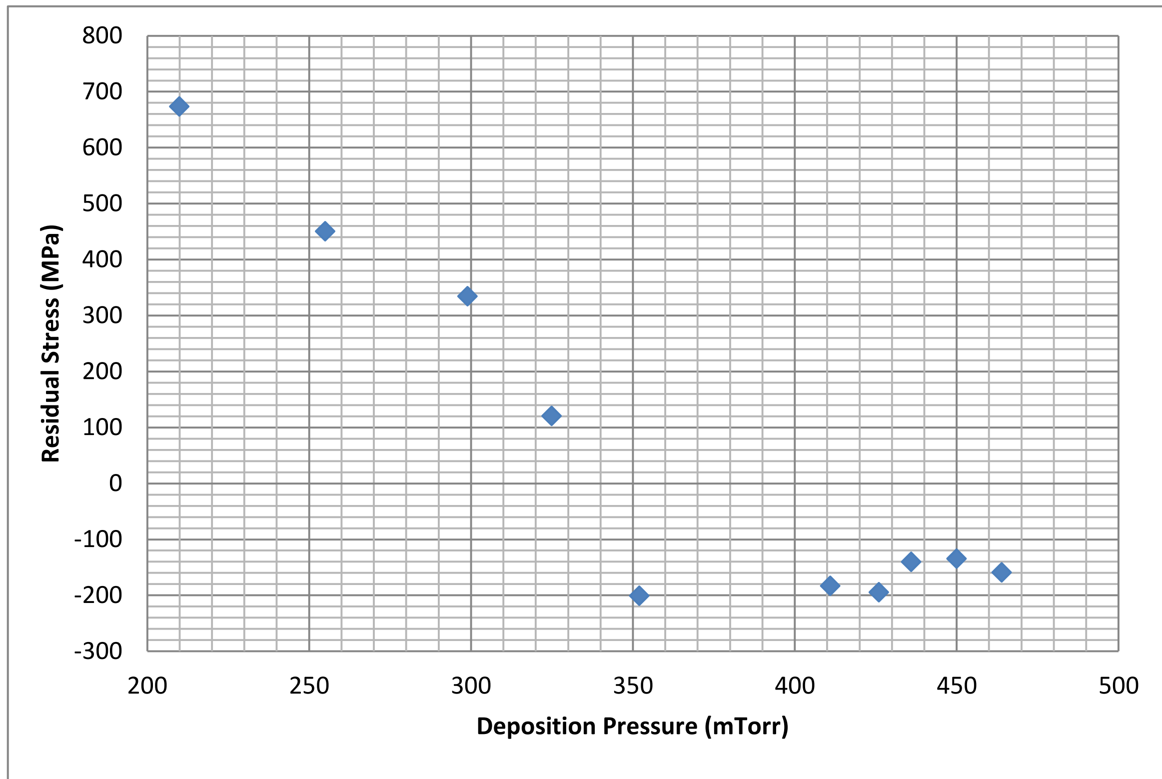

Figure 2.3: Residual stress of 3C-SiC films as a function of pressure

The residual stress of a polycrystalline thin film is a result of the difference in the coefficients of thermal expansion of the silicon substrate and the 3C-SiC film. At lower pressures, larger nucleation sites for 3C-SiC form, resulting in tensile films. The opposite occurs at higher deposition pressures; smaller nucleation sites form resulting in compressive films. The differences in nucleation rate are a result of the change in reaction thermodynamics caused by different pressures. The effect on mechanical properties due to film stress has not been investigated for the films grown at NCSU.

For the entire range of study, the only parameter of the process that is altered is the pressure. As mentioned previously, temperature is not changed because the equipment belongs to a shared use facility. Additionally, since the temperature cannot be changed, the gas flow rates also cannot be changed because the stoichiometry of process will change.

The mechanism for chemical vapor deposition of 3C-SiC is a chemical reaction which occurs when several precursor gases react in a low pressure environment to form 3C-SiC. Prior to performing LPCVD, 100 mm diameter <100> silicon substrates are cleaned of contaminates and spin dried prior to loading in the furnace as described in section 2.1. The wafers are then loaded on a quartz boat with backing wafers which prevent the growth of 3C-SiC on the back side of the wafers. Upon loading the furnace with wafers, the LPCVD chamber is typically pumped down over night to low pressures. The pump system present in the furnace allows for pressures as low as 215 mTorr (2.8×10^{-4} atm) up to approximately 500 mTorr (6.6×10^{-4} atm). The deposition pressures used for samples prepared in this study are 250 mTorr and 300 mTorr. Two different pressures were used in order to determine if small differences in film stress led to a significant change in electrical characteristics. Once the

furnace pumps down overnight to pressures in the mTorr range, the depositions are performed the following day.

The furnace present in the NCSU cleanroom is held at an ambient 400°C. Visual representations of the main steps which take place in the complete process flow are illustrated below in Figure 2.4 [17].

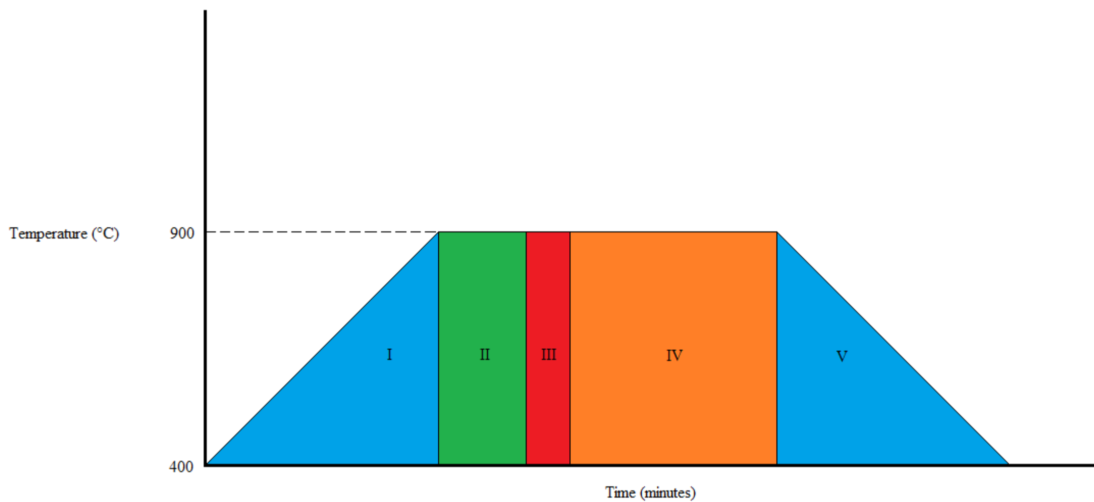

Figure 2.4: Visual Representation of the LPCVD Process used to Grow Poly 3C-SiC

- **I. Temperature Ramp up from 400°C to 900°C (100 Minutes)**
- **II. Temperature and Pressure Stabilization (20 Minutes)**
- **III. Carbon Layer Deposition (1 Min)**
- **IV. Main Deposition Step (50-90 Min)**
- **V. Temperature Ramp Down from 900°C to 400°C (60 Min)**

The first stage of the CVD process is a temperature ramp-up (I). This heating process takes 100 minutes in order for the furnace to reach the deposition temperature of 900°C. The second stage (II) of the process is furnace stabilization where the temperature reaches a

uniform 900°C and the pressure levels out to the desired deposition pressure. For doped films the deposition pressure is normally between 250 to 300 mTorr, since this range has been well characterized in terms of growth rate. The third stage (III) of the LPCVD process involves the deposition of a very thin layer of carbon which creates an adhesion layer for 3C-SiC growth on silicon; and improves deposition uniformity throughout the surface of the wafers. The carbon layer is deposited over a two minute time span where acetylene (C_2H_2) reacts with hydrogen gas (H_2) to form carbon on the surface of the wafer. This carbon deposition is generally performed at the same growth pressure as the silicon carbide film and takes one minute to complete. Once the short carbon coat step is complete, the main deposition step begins (IV). The deposition of 3C-SiC occurs when dual precursor gases of acetylene and DCS are flowed into the furnace and react to form the thin film [8]. In order to achieve an n-type film (excess donor sites), a low concentration of ammonia (NH_3) is introduced into the furnace and the film is in-situ doped with nitrogen [30, 35]. The resistivity of typical doped films is on the order of 0.02-0.04 Ω-cm. With the addition of ammonia into the process, a time of approximately 90-100 minutes is needed in order to achieve a film thickness of approximately 3000 Angstroms. Once the deposition step is complete, the final step (V) of the process involves a ramp down of the furnace to the nominal temperature of 400°C and a nitrogen purge to remove the DCS and acetylene from the furnace lines. The entire process typically takes between 6-8 hours but a large number of wafers can be run at the same time if necessary.

2.3 TEM Imaging of 3C-SiC

The silicon carbide produced using the LPCVD method described in the previous section has a unique structure. The 3C-SiC thin films are grown hetero-epitaxially on silicon substrates and form long columnar grains with varying thicknesses. The thickness of the grains depends on the growth pressure with tensile films having wider grains than compressive films. The grain structure and orientation of two 3C-SiC films grown at pressures of 225 MPa and 425 MPa respectively were investigated using a transmission electron microscope (TEM).

The 3C-SiC samples used to observe grain structure of the material were grown using the LPCVD procedure outlined in chapter 2 section 2. The samples were prepared using a focused ion beam (FIB) to carve out a thin portion of the film/substrate interface which could be observed in the TEM. The first sample observed was the 3C-SiC tensile film (Figure 2.5 below) grown at a furnace pressure of approximately 225 MPa [17].

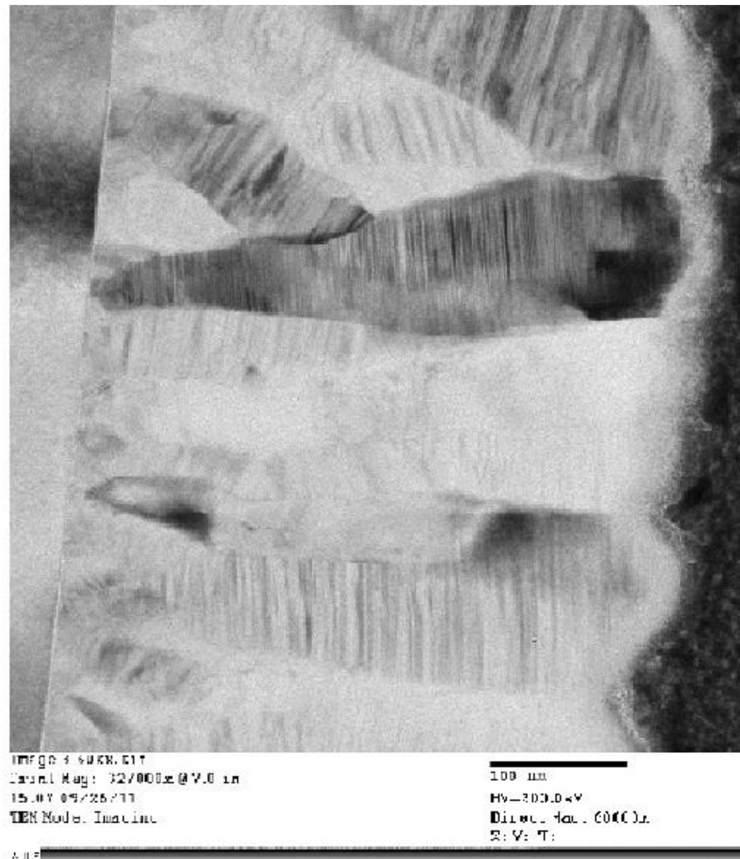

Figure 2.5: TEM Image of a Tensile 3C-SiC Thin Film at 40,000x

The TEM image of the tensile film demonstrates the columnar grain structure present in the 3C-SiC. Tensile silicon carbide films such as the sample illustrated in Figure 2.5 is the subject of investigation in this report. Several grains run the length of the film and are various widths. The lines which run across the width of the grains are stacking faults in the structure of the silicon carbide. The stacking faults are imperfections in the ABCABC stacking sequence of 3C-SiC. These imperfections are a result of the silicon carbide growth process. Defects such as stacking faults are imperfections which hinder the performance of

devices fabricated using the material. This is the reason polycrystalline materials in general are not used by industry to fabricate electrical devices. Like the tensile film, the compressive 3C-SiC thin film displays similar columnar grains with the presence of stacking faults.

A compressive 3C-SiC film (grown at 450MPa) was compared to the tensile film. The compressive 3C-SiC TEM sample was prepared using a FIB like the tensile sample. The TEM image taken of the compressive film can be seen below in Figure 2.6 [17]. Both images were taken at 40,000x magnification.

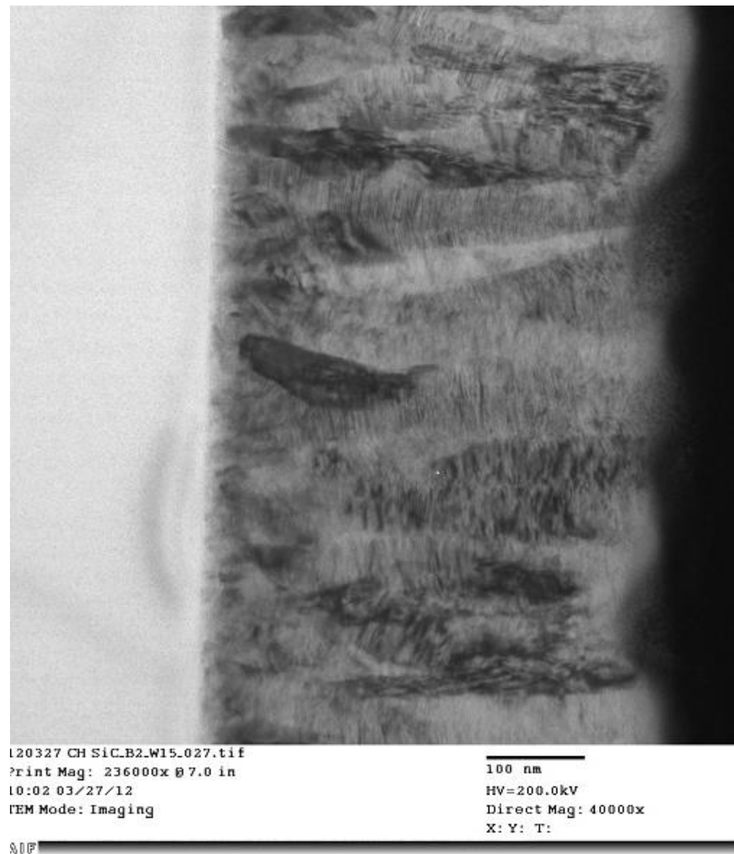

Figure 2.6: TEM Image of a Compressive 3C-SiC Thin Film at 40,000x

There are noticeable differences between the images of the tensile and compressive 3C-SiC. The columnar grains in the compressive film appear to be more densely packed than the grains of the tensile sample. Due to the tighter arrangement of grains, the individual grains appear to be smaller in the compressive sample than the grains of the tensile film. Like the tensile sample illustrated in Figure 2.5, the compressive grains contain numerous stacking faults which run the width of the entire grain.

2.4 Resistivity Samples

In order to create 3C-SiC samples for the measurement of electrical resistivity, a layer of 3C-SiC is grown on silicon dioxide in order to electronically isolate the thin film from the silicon substrate. There are two methods for oxidation which are employed; dry and wet oxidation. The method used in order to form oxide for the electronic isolation of the SiC thin films is dry oxidation performed at 950 °C. Despite the fact that wet oxidation is a quicker process, dry oxidation is chosen because the density of the oxide layer is greater resulting in a better isolation layer [5]. In order to achieve appropriate isolation, 500 Angstroms of SiO_2 is deposited on 100 mm, <100> oriented, 500μm thick silicon substrates. All wafers are cleaned (RCA bath and buffered oxide etch) and spin dried before being loaded in the oxidation furnace. The depositions are performed in a low pressure chemical vapor deposition furnace using O_2 and HCl gases as precursors at the specified temperature. The furnace configuration is similar to the furnace used to grow 3C-SiC [31]. The design of the furnace and heating source allows for temperature uniformity on the order of +/- 0.1°C.

Throughout all oxidation runs the temperature is monitored at three different points in the furnace to ensure a uniform deposition.

The oxygen is the primary gas which reacts with the silicon from the substrates to form the SiO_2 layer. The reaction is described by the formula:

$$Si + O_2 \rightarrow SiO_2$$

The HCl gas in the process serves several purposes including the removal of any metal ions which may be present on the Si substrates and to keep the furnace and furnace pipes clean of the O_2 gas. With the details of the oxide growth known, several concepts can be applied in order to determine oxidation time and the amount of Si consumed during the process.

The growth rate of SiO_2 in the NCSU Nanofabrication facility (NNF) furnace has been characterized by the staff using the average oxide thicknesses from various furnace runs at various run times. The model used to characterize the data is the commonly used Deal-Grove model. The data is summarized and fit with a polynomial equation in Figure 2.7 below [5,16]. With the exception of a few samples, the data has tracked with the parabolic relationship fairly well indicating the accuracy of the model.

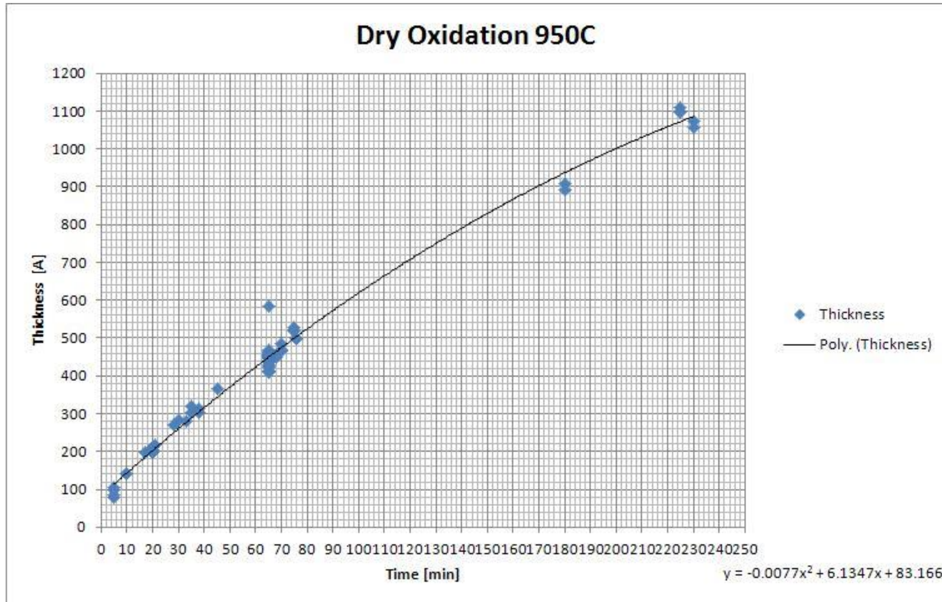

Figure 2.7: Oxide Thickness vs. Time at 950°C for the NCSU NNF Dry Oxidation Process

As evident from the above plot, the growth rate of SiO_2 is governed by a parabolic growth rate. Based on previously collected data, the growth time needed in order to achieve the desired 500 Angstroms of SiO_2 is approximately 75 minutes. With this data the growth rate is determined to be 0.111 Angstrom/sec (6.667 Angstrom/min). After the 75 minute deposition at 950 °C, the thickness of the SiO_2 was measured using a Nanometrics® reflectometer. The thickness of the oxide layer varied no more than 5 Angstroms across the surface of each wafer. Using five data points, the thicknesses of the SiO_2 layer on five wafers was measured and averaged together. These thicknesses are listed below in Table 2.1.

Table 2.1: Thickness of SiO_2 Layers on Five Silicon Wafers after Oxidation

Wafer	Oxide Thickness (A)
1	518.6
2	520.5
3	519.6
4	518.2
5	517.4

Once the isolation layer of silicon dioxide was grown on the wafers, a LPCVD deposition of n-type 3C-SiC was performed using the procedure outlined in section 2.2. In addition to being used for resistivity measurements, the 3C-SiC on SiO_2 wafers were also used as monitors for determining the resistivity of the 3C-SiC layers grown on bare silicon wafers. These values are important for the determination of p-n junction parameters. The monitor wafers used to determine the resistivity of the thin films grown on bare silicon substrates were used as the samples for the resistivity tests. Information including film resistivity and thicknesses for two runs will be described in the following section. The final structure of the monitor wafers used for resistivity measurements is illustrated below in Figure 2.8.

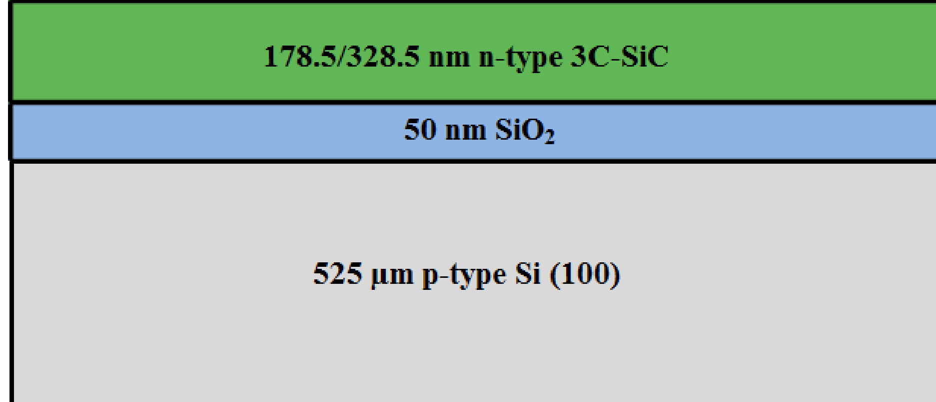

Figure 2.8: Illustration of Sample used for Resistivity Measurements

Two separate 3C-SiC runs were used to create these samples. The conditions will be described in section 2.5 as they are the same values used to grow SiC for the creation of p-n junctions. A flow chart (Figure 2.9) describing the fabrication steps of both the resistivity samples and the p-n junctions present in the following section.

2.5 Fabrication of p-n Junctions

There are several methods used to create a p-n junction. The most common method for fabricating a p-n junction is to dope an n-type substrate with a p-type dopant to create an interface of the materials with mismatched majority carrier charge polarity. This process typically involves taking a substrate (n-type), performing ion implantation or thermal diffusion (of a p-type dopant) to introduce the dopants, then to anneal the doped material in order to diffuse the dopant to achieve the desired dopant profile [7]. The annealing also

serves to electrically activate the dopant in the material so that the material responds to an electrical stimulus. In the case of doping silicon carbide, there are problems which arise which prevent the use of this commonly used method. Doping via ion implantation and electrically activating the dopants in 3C-SiC is difficult due to the extreme temperature needed to achieve activation. In one such study investigating doping profiles in 3C-SiC, an annealing temperature in the excess of 1600°C is needed to activate 1% of the dopants [39]. This annealing temperature is unattainable at the NCSU facilities, and additionally, the required annealing temperature is much larger than the melting temperature of silicon (1400°C), which is the substrate being used for 3C-SiC growth. Due to the limitations of attainable temperature at the NCSU facilities, alternative methods of forming p-n junctions from 3C-SiC were investigated.

A second method of method of forming a p-n junction is through the epitaxial growth of p-type and n-type layers on a substrate. This procedure is commonly performed in industry and for research purposes for extreme environment application. Given the difficulty of electrically activating dopants as explained previously, this method has been used for the formation of research grade SiC diodes. For example, NASA has fabricated high performance diodes out of 6H and 3C-SiC on 6H SiC substrates. These diodes are comprised of layers of n-type and p-type SiC with various doping concentrations stacked on each other. Despite the high performance of these diodes, the procedure is impractical for fabrication in the NCSU cleanroom since the furnaces cannot reach the required temperatures used by NASA and in industry. The devices fabricated at NCSU for this study were formed by

growing n-type 3C-SiC on p-type silicon substrates. The procedure for forming these structures is adopted from a procedure outlined by Chung et al [9, 10].

The processes used to fabricate both the resistivity samples and the p-n junctions involved several of the same steps. In both cases the wafers were cleaned of contaminates and native oxides using an RCA bath and buffered oxide etch respectively, then spin dried. The 3C-SiC was grown on both the silicon and oxidized wafers using the same two run conditions used to deposit the 3C-SiC for p-n junctions. After the LPCVD step, the p-n junction samples had aluminum and gold contacts deposited using resistive heating evaporation and DC sputtering respectively. Following the deposition of contacts, the wafers were cleaved and electrically characterized. This entire procedure is outlined in the following flow chart (Figure 2.9) and will be described in greater detail in this section.

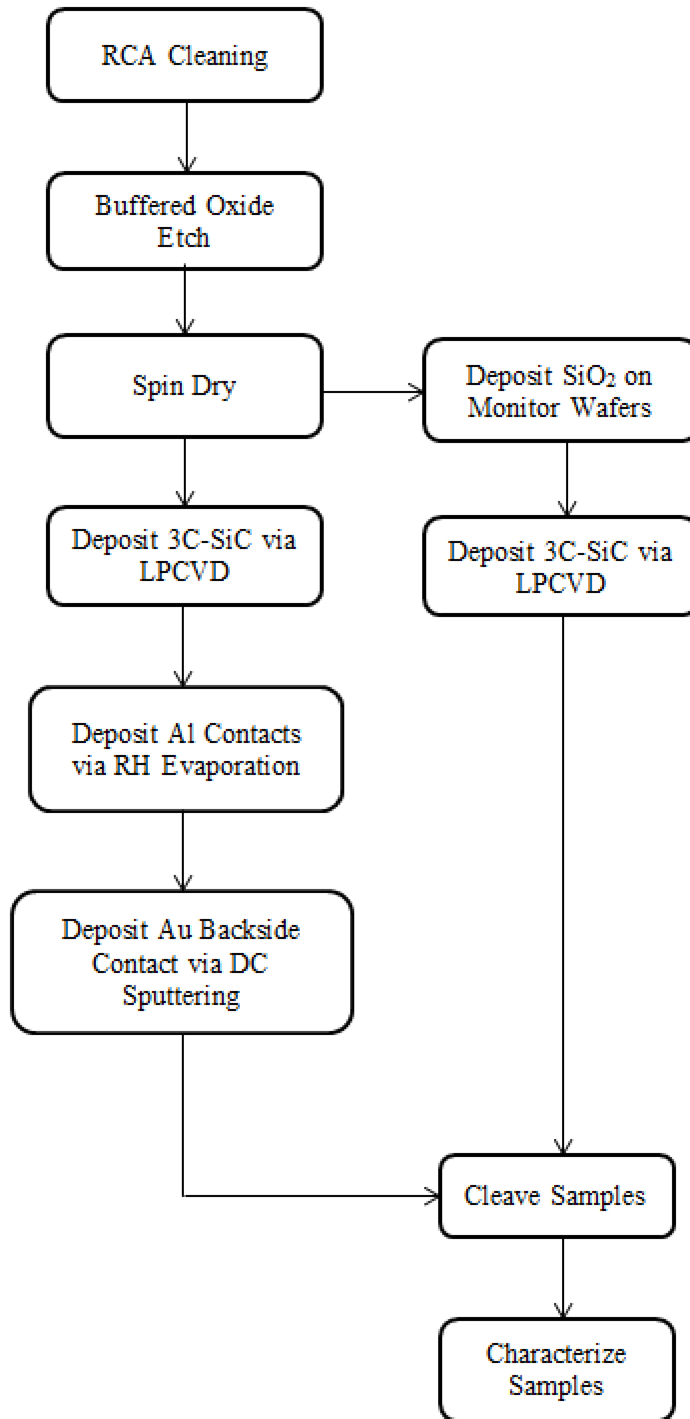

Figure 2.9: Flowchart Outlining the Procedure used to Fabricate Resistivity and p-n Junction Samples

The first step taken to fabricate diodes from 3C-SiC was the obtainment of silicon substrates with the desired p-type doping concentration. Since it is desired to observe the damage in the SiC rather than the silicon, a low resistivity substrate (relative to the 3C-SiC) is necessary to ensure the depletion region in the device is primarily in the 3C-SiC by volume. In this case, the resistivity of the silicon should be on the order of 0.002 Ω-cm since the resistivity of the 3C-SiC grown in the NCSU clean room is on the order of 0.02 to 0.04 Ω-cm. With the appropriate resistivity substrate, n-type 3C-SiC is then grown on the silicon substrates via chemical vapor deposition. This procedure is performed in a furnace at 900°C by flowing the gases outlined in section 2.2. Again, the n-type dopants are introduced by the addition of ammonia gas to the process. The nitrogen in the ammonia is the n-type dopant. Once 3C-SiC is grown on the silicon, ohmic contacts are placed on the silicon substrate and the 3C-SiC layer in order to provide optimal current flow through the device. The contact placed on the silicon substrate is gold, which is sputtered on the surface. The contact on the 3C-SiC is aluminum which is evaporated onto the surface. This completed device will provide a structure creating an IV curve with the desired properties resulting from mostly the silicon carbide.

The structure of a p-n junction is simple as it consists of an interface of materials, one with a dominant n-type concentration, and the other with a dominant p-type concentration. The area near the interface of the materials is known as the depletion region, which devoid of mobile charge carriers due to n-type and p-type carrier recombination. The lack of mobile charge carriers generates an internal electric field caused by the internal fixed charge from

the valance mismatched dopants in the lattice as well as any external applied potential in the p-n junction. This built in potential is given by the equation [53]:

$$\phi_1 = V_t \frac{p_n * n_p}{n_{Si} * n_{SiC}} \qquad \text{Eq. 2.2}$$

Where p_n is the number of p-type acceptors, n_p is the number of n-type donors, n_i is the intrinsic concentration of the material, and V_t is the thermal voltage of 0.026V. The thermal voltage is a temperature dependent parameter equal to the product of the Boltzmann constant and temperature, divided by the charge of an electron. With the built in potential known, the width of the depletion region in the p-n junction is given by [53]:

$$x_d = \sqrt{\frac{2\varepsilon_s}{q} * \left(\frac{1}{N_a} + \frac{1}{N_d}\right) * (\phi_1 - V_a)} \qquad \text{Eq. 2.3}$$

The terms in this relation are: the dielectric constant of the material ε_s, q is the charge of an electron (1.602×10^{-19} C), N_a and N_d are the volumetric concentration of acceptors and donors, while V_a is the applied potential in volts. With the width of the depletion region known, the fraction of this region in the n-type and p-type material can be calculated using the ratio of number of donors and acceptors. The ratio of the depletion region in the n-type material is:

$$x_n = x_d * \frac{N_a}{N_a + N_d} \quad \text{Eq. 2.4}$$

While the ratio of the depletion region in the p-type material is:

$$x_p = x_d * \frac{N_d}{N_a + N_d} \quad \text{Eq. 2.5}$$

As evident from the above relations, the depletion region will tend to be larger in the material with a smaller concentration of acceptors or donors [53]. Since the structures being formed are comprised of both silicon and SiC, and the material of interest is the SiC, the desired depletion region should lie mostly in the 3C-SiC. In order to achieve a majority depletion region in the n-type 3C-SiC, the concentration of acceptors in the silicon substrates should be approximately an order of magnitude larger than the concentration of n-type donors in the 3C-SiC.

The number of dopants in the SiC is proportional to the ammonia flow in the CVD process used to grow the 3C-SiC. At current settings in the NCSU cleanroom, the maximum ammonia flow of 90 sccm yields a donor concentration on the order of 10^{18} per centimeter cubed. The number of donors in the n-type SiC and acceptors can be calculated using the known resistivity of both the 3C-SiC thin film and the silicon substrates. The resistivity of the 3C-SiC can be determined by performing a four point probe measurement of the

$SiC/SiO_2/Si$ stack. The following equation represents the relation of resistivity to the number of number of donors/acceptors.

$$n = \frac{1}{q\rho\mu} \quad \text{Eq. 2.6}$$

In equation 2.6, q is the charge of an electron, ρ is the material resistivity (in Ω-cm), and μ is the mobility ($cm^2/(V*s)$) of donors/acceptors in the given material [22]. With equations 2.2 to 2.6, p-n junction diodes can be designed to provide electrical feedback for measuring radiation damage in 3C-SiC.

The creation of p-n junctions was performed under two different processing parameters. All wafers were prepared according to the procedure in section 2.1, with monitor wafers undergoing an oxidation processes in order to electronically isolate the 3C-SiC thin films for resistivity measurements. The two runs performed to create p-n junctions were performed at different growth pressures, varying ammonia flow, and for different times. The details including final thin film thickness are displayed below in Table 2.2.

Table 2.2: Process Conditions used for p-n Junction and Resistivity Samples

Run	Time (min)	Growth Pressure (mTorr)	Ammonia Flow (sccm)	Final Film Thickness (nm)
1	50	250	90	178.5
2	90	300	60	328.5

The growth rate of 3C-SiC is dependent on all the parameters listed above with time having the largest effect and ammonia flow having the smallest. Two different runs were performed in order to determine the effect of pressure on electrical response of the 3C-SiC. The film deposited in run two was performed at 60 sccm so that a thicker film with an equivalent resistivity to the film grown in run one could be obtained. With two samples with similar resistivities, the effect of film thickness on the accumulation of radiation damage could be determined. Following the processing, the thicknesses of the films are determined using a Nanometrics® reflectometer and the resistivities are determined using a four point probe.

With the thicknesses and resistivities of the films known, the number of donors and acceptors in the 3C-SiC and silicon thin film can be determined respectively. For the determination of substrate resistivity a thickness of 525 µm was used. Another piece of information needed to determine the acceptor/donor concentration was the mobility of holes in silicon and the mobility of electrons in 3C-SiC. The mobility of holes in silicon was estimated to be 100 $cm^2/V*s$ since the hole mobility of silicon tends to decrease as the dopant concentration increases. Silicon with a very small sheet resistance tends to acceptor concentrations on the order of $10^{19}/cm^3$ to $10^{20}/cm^3$ thus a small hole mobility [7, 22]. The electron mobility of single crystalline 3C-SiC with a dopant concentration of $10^{16}/cm^3$ is approximately 800 $cm^2/V*s$. Since the mobility decreases as the number of defects increases, the mobility of polycrystalline 3C-SiC will be much smaller than that of single crystalline 3C-SiC. An electron mobility value of 120 $cm^2/V*s$ was approximated [12]. Using the known information, the concentration of donors and acceptors was determined using equation 2.6. The results are summarized below in Table 2.

Table 2.3: Resistivities, Mobility, Acceptor Concentration, and Donor Concentration for Si and 3C-SiC

Run	Substrate Resistivity (Ω-cm)	Hole Mobility of Si ($cm^2/V*s$)	Acceptor Concentration (cm^{-3})	Film Resistivity (Ω-cm)	Electron Mobility of SiC ($cm^2/V*s$)	Donor Concentration (cm^{-3})
1	0.0036	100	$1.734x10^{19}$	0.0311	120	$1.638x10^{18}$
2	0.0034	100	$1.836x10^{19}$	0.0346	120	$1.503x10^{18}$

With the concentrations of donors in 3C-SiC and acceptors in Si known, parameters of p-n junction diodes can be determined. Equations 2.2 to 2.6 are used in order to determine the parameters of the p-n junctions with the percentage of the depletion region in the SiC being the most important parameter. With a depletion region mostly in the 3C-SiC rather than the silicon, the IV curves generated will represent how the characteristics of the SiC change as opposed to the silicon.

The first value calculated is the built in potential of the p-n junction as represented by equation 2.2. The built in potential is a function of the number of donors, acceptors, and the intrinsic doping concentration of the 3C-SiC. The number of donors and acceptors is listed in Table 2.3, the intrinsic carrier concentration of SiC is 0.15 carriers per centimeter cubed [4] and the intrinsic concentration value for silicon is 10^{10} carriers per centimeter cubed, and the thermal voltage is 0.026V. With this value the width of the depletion region is determined at a potential of 0V. With a known depletion region thickness, the percentage of this region in each material can be determined. These results are calculated and listed below in Table 2.4. It should be noted that these built in potential values will not be visible in the experimental I-V characteristics measured. The built in potential values listed in Table 2.4 assume crystalline materials, and do not account for defects present in the 3C-SiC. Single crystalline 3C-SiC was assumed in order to approximate the percentage of the depletion region in the polycrystalline 3C-SiC films.

Table 2.4: p-n Junction Parameters

Run	Built in Potential (V)	Depletion Region Thickness at 0V (nm)	Percentage of the Depletion Region in the SiC
1	2.336	44.901	90.836
2	2.334	47.084	91.851

With an acceptable depletion region of the p-n junction located in the 3C-SiC, the final step required to characterize the devices are the placement of front and backside contacts on the 3C-SiC and silicon respectively.

The placement of contacts on the p-n junctions was performed using two PVD deposition techniques. The goal of contact placement is to create ohmic contacts on each side of the devices which would allow for easy probing and current flow through the materials. Gold and aluminum were determined to be the best ohmic contacts for silicon and gold respectively by Chung et al [11]. The contacts placed on the 3C-SiC were aluminum deposited via RH (resistive heating) evaporation. The RH evaporation system used for this procedure located in the NCSU cleanroom is pictured below.

Figure 2.10: Resistive Heating Evaporator Located in the NCSU Cleanroom [5]

The procedure was performed at a pressure of approximately $2x10^{-6}$ Torr in a vacuum chamber. The source of aluminum were pellets placed in a tungsten boat which was heated by running high current through the boat until the pellets became molten, evaporated, and coated the suspended wafers [1, 31]. Round contacts 1 mm in diameter were obtained by placing a shadow mask on the suspended wafers. The thickness of the aluminum was determined by performing profilometry measurements and averaging the values on a monitor wafer placed alongside the 3C-SiC wafers. The average aluminum layer thickness was approximately 150 nm and this value was then used for determining damage profiles on the

samples as described in chapter 3. Once the aluminum contacts were placed on the 3C-SiC side of the wafers, gold was deposited on the silicon side to create a backside ohmic contact.

The procedure for depositing gold on the silicon was different than the procedure used to deposit aluminum because gold pellets were not available. Instead, a DC sputtering system (pictured below [5]) was used to do so.

Figure 2.11: DC Sputtering used to Deposit Gold Contacts

The DC sputtering procedure was performed in two steps; first a thin layer of titanium was deposited on the Si to create an adhesion layer and then the gold was deposited on top of the titanium. For the DC sputter deposition, two targets; one gold and one titanium are placed inside a vacuum chamber with the suspended wafers rotating above the two targets. The sputtering process is performed by creating a plasma in the chamber which bombards the

titanium and gold targets with ions, ejecting atoms from the targets onto the silicon [1, 46]. The titanium was deposited first and the layer placed on the silicon was approximately 20 nm thick. Following the deposition of the adhesion layer, the gold was then sputtered onto the adhesion layer of titanium. Using a profilometry measurement of a glass slide placed in the chamber, it was determined that the thickness of the gold layer deposited was approximately 200 nm thick. The final profile on the p-n junctions is illustrated below in Figure 2.12

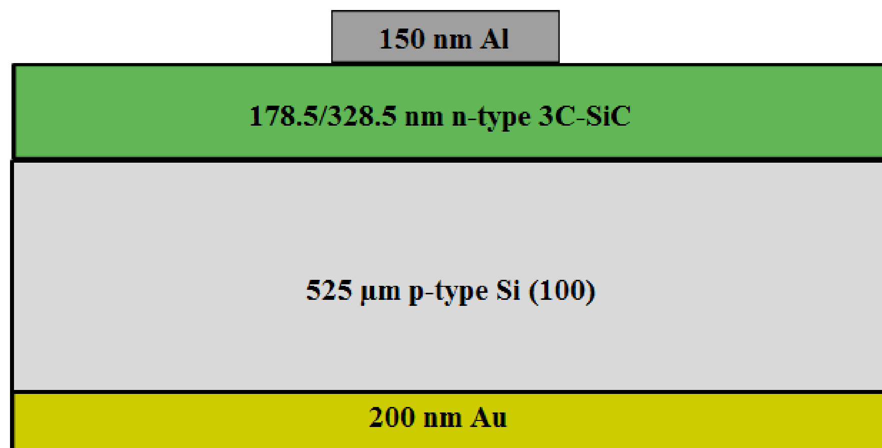

Figure 2.12: Cross Section of the p-n Junction Structure

Following the deposition of the gold contact, the fabrication of the p-n junctions was complete. The wafers were then cleaved into 1 cm x 1 cm pieces which were then characterized electronically, irradiated, and characterized again. This procedure will be outlined in the following chapters.

Chapter 3

Device Irradiation

3.1 Ion Beam System

The goal of the 3C-SiC investigation is to better understand the onset of radiation damage and the evolution of defects in the material as it is being irradiated. Materials used in nuclear reactor applications are subject to neutron irradiation as they are the product of the nuclear fuel fission. North Carolina State University houses a 1 MW test nuclear reactor which is capable of irradiating materials but there are some problems associated with using this system as a source of irradiation. The current configuration of the system places test samples far from the core of the reactor resulting in long irradiation times required to achieve damage levels of fractions of dpa. For the study of 3C-SiC, a wide range of damage levels are desired for investigation. The test reactor cannot provide timely irradiation of the 3C-SiC as in some instances, months are required for high dose irradiations. In addition to the long irradiation times, a future goal of this work is to perform in-situ characterization of 3C-SiC. In-situ methods cannot be applied to the nuclear reactor since it is not possible to contact the samples while they are being irradiated. With the required irradiation conditions and goals of the study, an alternative method of irradiating the 3C-SiC samples are required.

Ion beam irradiation is a commonly used method of irradiating materials since a large range of damage levels can be achieved in a relatively short period of time. Additionally, an

ion beam system would be much easier to configure for making in-situ measurements of samples. There are a number of ion beam systems available including facilities at Sandia National Laboratory and at Pacific Northwest National Lab. For this study, a newly constructed ion beam system (Figure 3.1) at the University of Tennessee in Knoxville (UTK) will be utilized.

Figure 3.1: Ion Beam System at the University of Tennessee in Knoxville [47]

The system is capable of delivering a wide range of ion fluence damage in materials with various types of ions. The irradiations performed on 3C-SiC samples will utilize silicon ions since they will not alter the chemical make-up of the samples. Further details of the irradiations, including simulations will be described in the following sections.

3.2 Sample Mounting and Irradiation Conditions

The ion beam system is comprised of numerous components including an ion source at the front, accelerator tube in the center, and vacuum chamber at the end. The vacuum chamber at the end of the system is the location where the samples were housed for irradiation studies. The chamber (pictured below), has a holder inside it which allows for mounting of the samples in line with the ion beam.

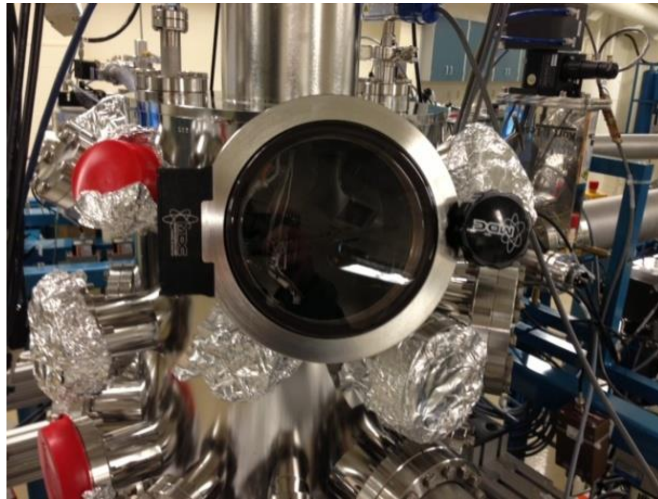

Figure 3.2: Vacuum Chamber which Housed the Samples to be Irradiated

In order to perform irradiation experiments, the chamber is pumped down to pressures of approximately 10^{-7} Torr. Each individual sample was cleaved into a 1cm x 1cm square and stuck onto a stainless steel slat (Figure 3.3) with double sided carbon tape. In addition to the samples, pieces of reflective glass were also placed on the slat which allowed beam operators to locate the beam and direct it onto the samples.

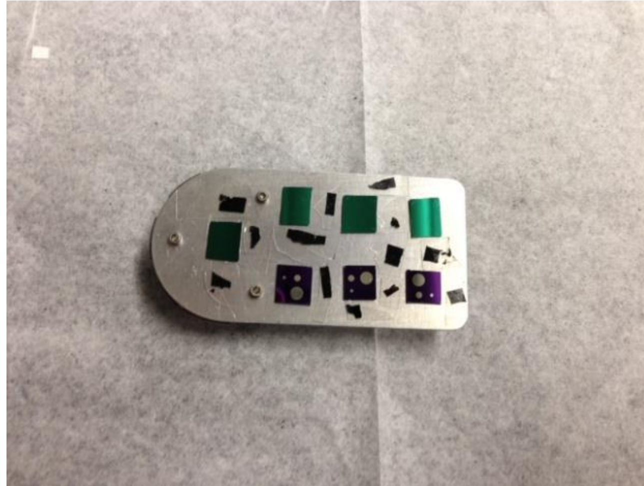

Figure 3.3: Stainless Steel Slat that Samples were Mounted on

The stainless steel slat had a connector on the back which hooks into the vacuum chamber. Once the sample mount was placed in the chamber and it pumped down, the irradiations were performed.

The ion beam system can be configured to perform irradiations with a variety of ions. Silicon ions with an energy of 1 MeV will be used for the irradiation of 3C-SiC samples. The ion fluence each sample is irradiated with is directly related to the time exposed to the ion beam. The lowest ion fluence used was $5x10^{12}$ ions/cm^2 and the highest fluence was $1x10^{15}$ ions/cm^2. Irradiation times can range from a few 10's of seconds to over an hour per sample, depending on the ion fluence. There were two sets of experiments performed, tests on resistivity samples, and tests on p-n junctions. The tests were repeated twice, once on the samples with a 178.5 nm thick film, and again on the samples with a 328.5 nm thick film. The target fluences for irradiating the resistivity samples are listed below in Table 3.1.

Table 3.1: Target Fluences for Resistivity Samples

Experiment	Target Fluence (ions/cm^2)
1	$5x10^{12}$
2	$7.5x10^{12}$
3	$1x10^{13}$
4	$2.5x10^{13}$
5	$5x10^{13}$
6	$1x10^{14}$
7	$5x10^{14}$
8	$1x10^{15}$

Fewer fluence conditions were considered for p-n junction irradiations. The experiments are listed below in Table 3.2.

Table 3.2 Target Fluences for p-n Junction Samples

Experiment	Target Fluence (ions/cm^2)
1	$5x10^{12}$
2	$5x10^{13}$
3	$5x10^{14}$

3.3 Irradiation Simulations using TRIM Software

There are numerous tools available for the simulation of ion damage in silicon carbide such as Molecular Dynamics (MD) simulations. The damage created by silicon ions in the Al/SiC/Si/Au and SiC/SiO_2/Si structures is simulated using a software package called The Range of Ions in Matter (TRIM). TRIM software provides a number of options for simulating the damage of ions in matter including irradiation ion species and ion energy. TRIM also allows the user to select materials parameters for the target materials including thicknesses and chemical make-up of each material [54]. With the structure of each material known, including material thickness, TRIM can simulate the range of the ions in the material stacks and display the location of damage peaks resulting from the irradiations. TRIM simulations will be provided for each irradiation condition on each sample.

The first structure simulated using TRIM software was for the SiC/SiO_2/Si structure illustrated previously in Figure 2.8. The simulations were performed twice, once for a 178.5 nm thick film, and again for 328.5 nm film. The conditions of the simulations are kept the same for all sample configurations. Ion distribution profiles were created for the implant of 1000 silicon ions with 1 MeV of energy. The simulations demonstrated the path of each ion in the samples, the peak damage location, and the number of collision events using the Kinchen-Pease model [32, 54]. The first two figures below illustrate the paths of 1000 ions accelerated into SiC/SiO_2/Si with varying 3C-SiC thicknesses of 178.5 and 328.5 nm.

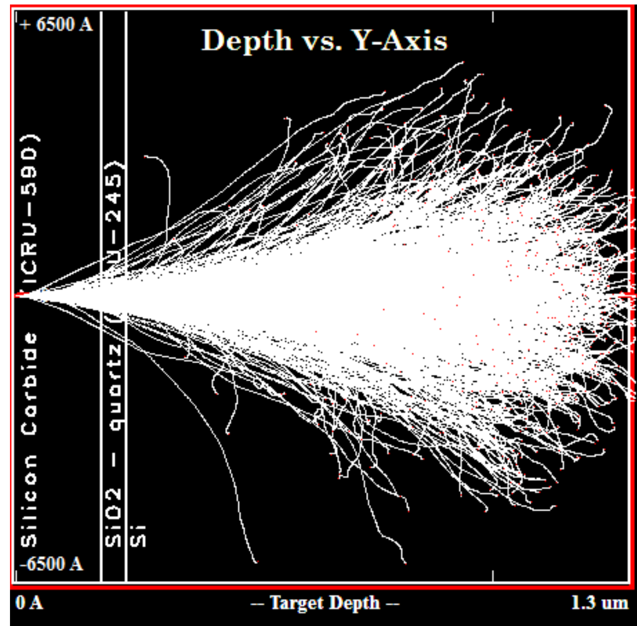

Figure 3.4: Depth vs. Y-axis for SiC(178.5 nm)/SiO_2/Si Structure

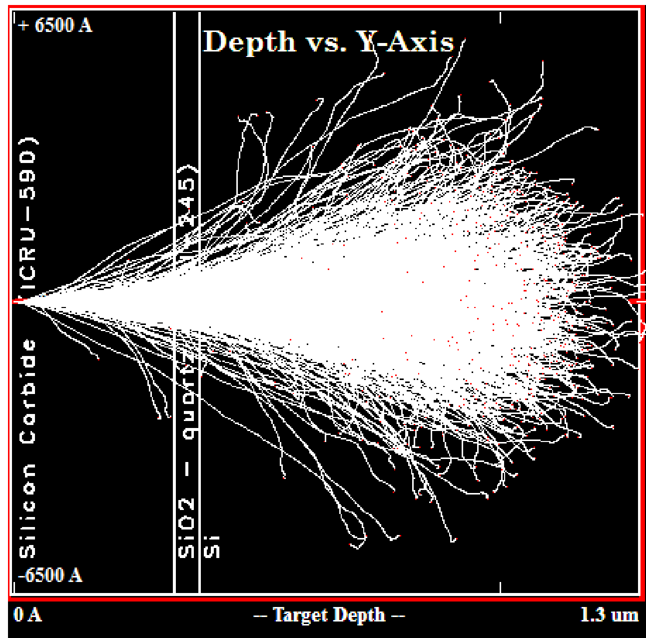

Figure 3.5: Depth vs. Y-axis for SiC(328.5 nm)/SiO_2/Si Structures

The depth versus Y-axis figures above illustrates the path of each ion as it is implanted into the $SiC/SiO_2/Si$ structures. There are not many observable differences between the profiles of the two sample thicknesses. A small number of ions stop in the thicker films. This result is demonstrated in the following two plots which illustrate the distribution of ion depths.

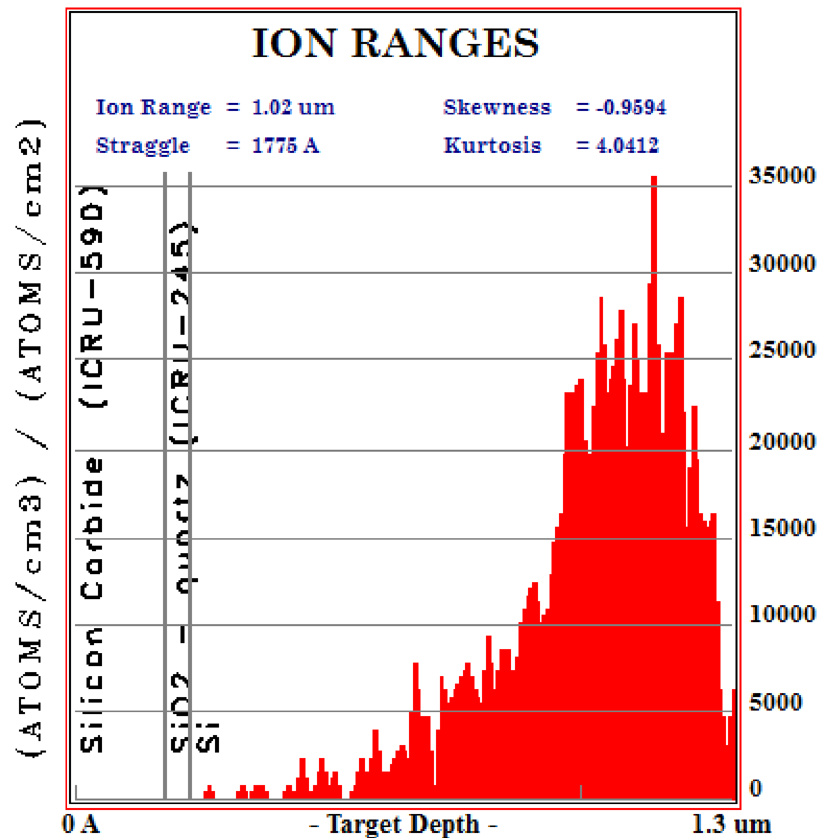

Figure 3.6: Ion Ranges for 1 MeV Ions into SiC(178.5 nm)/SiO_2/Si

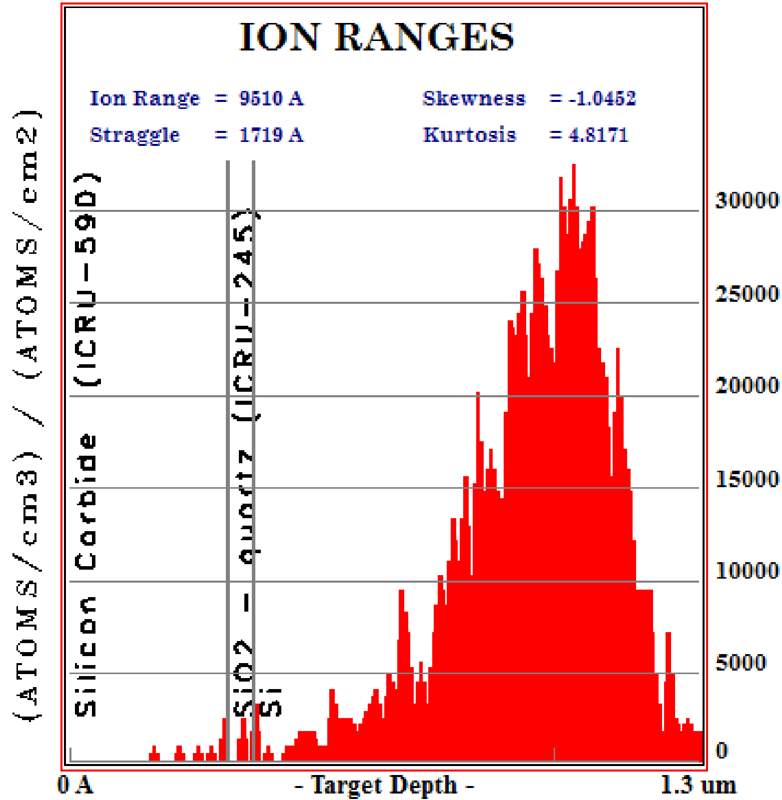

Figure 3.7: Ion Ranges for 1 MeV Ions into SiC(328.5 nm)/SiO_2/Si

The average range of a 1 MeV silicon ion implanted into the SiC/SiO_2/Si structure is 1.02 µm when the 3C-SiC thickness is 178.5 nm. The average range decreases to .951 µm when the 3C-SiC thickness is 328.5 nm. Inspection of Figure 3.7 indicates a small number of intersitials resulting from silicon ions stopping in the 328.5 3C-SiC film.

TRIM is also used to determine the number of collision events occuring in each layer of the SiC/SiO_2/Si structures. Figures 3.8 and 3.9 display the number of vacancies created by each incoming ion. The software applies the Kinchen-Pease model [32] to in order

determine the number of vacancies created in each material. The number of vacancies produced due to each ion is an important parameter because it indicates the amount of damage accumulating in the 3C-SiC thin film. These values will also useful for determining the dpa in each sample.

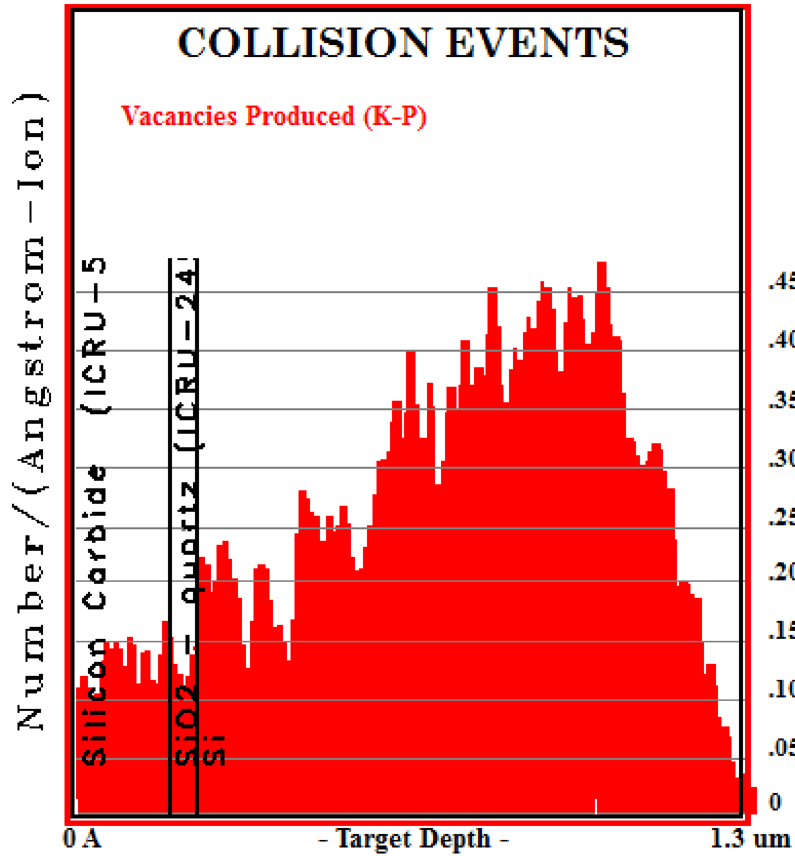

Figure 3.8: Collision Events for 1 MeV Ions into SiC(178.5 nm)/SiO_2/Si

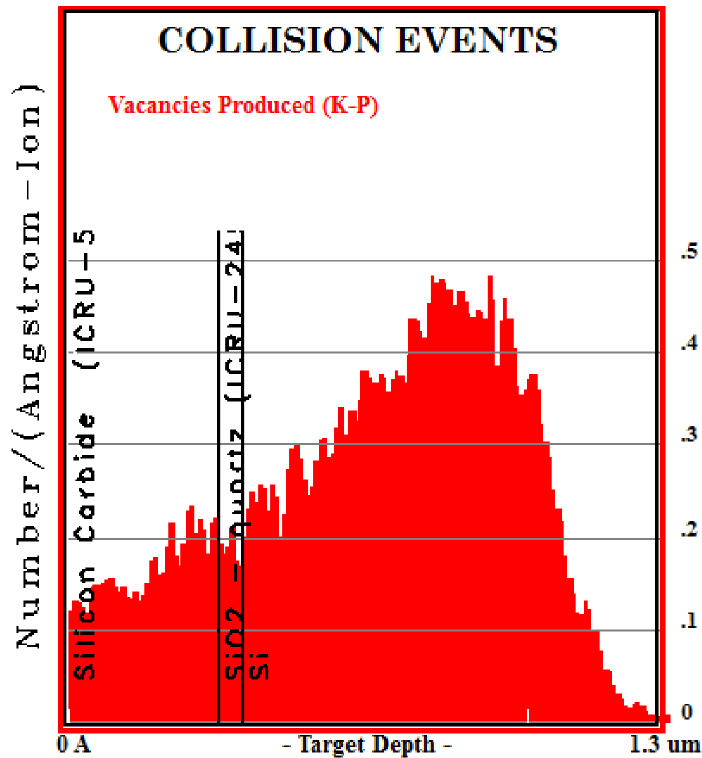

Figure 3.9: Collision Events for 1 MeV Ions into SiC(328.5 nm)/SiO_2/Si

The second set of TRIM simulations is performed for the p-n junction structure illustrated in Figure 2.12 with two different 3C-SiC film thicknesses. The conditions for the second set of irradiation simulations are the same as the conditions used for the SiC/SiO_2/Si simulations. The major difference between the simulations for the p-n junctions versus the resistivity samples is the presence of aluminum contacts on the diodes. This additional layer will dissipate energy from the 1 MeV silicon ions before they reach the 3C-SiC film resulting in smaller ion ranges compared to the previous set simulations. The first two plots illustrate the trajectory of 1 MeV silicon ions implanted into Al/SiC/Si structures.

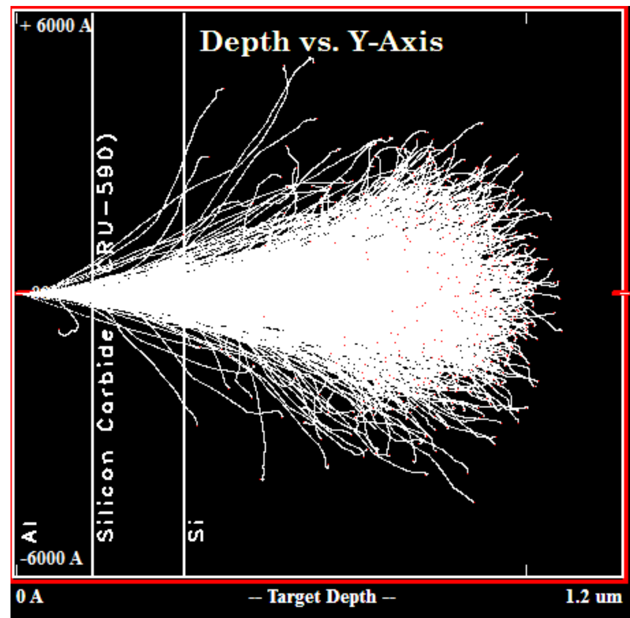

Figure 3.10: Depth vs. Y-axis for Al/SiC(178.5 nm)/Si Structure

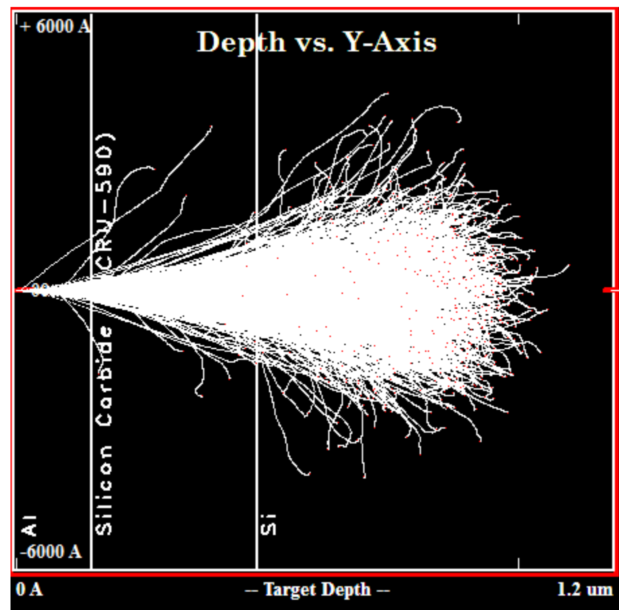

Figure 3.11: Depth vs. Y-axis for Al/SiC(328.5 nm)/Si Structure

It is evident that from inspecting Figures 3.10 and 3.11 that the aluminum contacts dissipate energy from the silicon ions before they reach the silicon carbide layer. Shorter ion ranges result due to the presence of aluminum layer. This assumption is confirmed by the ion range plots.

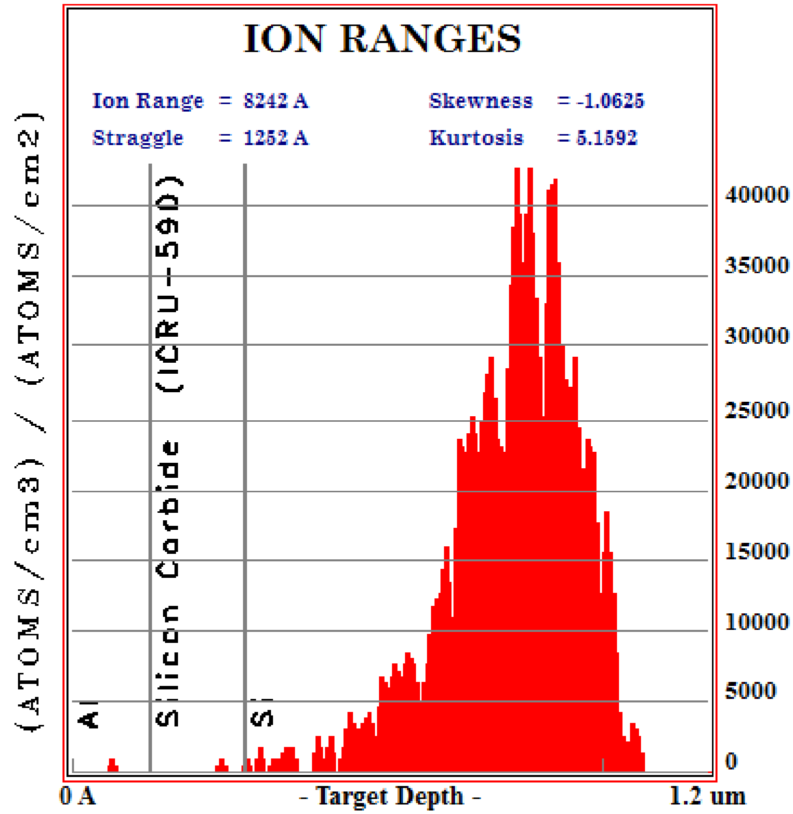

Figure 3.12: Ion Ranges for Al/SiC(178.5 nm)/Si Structure

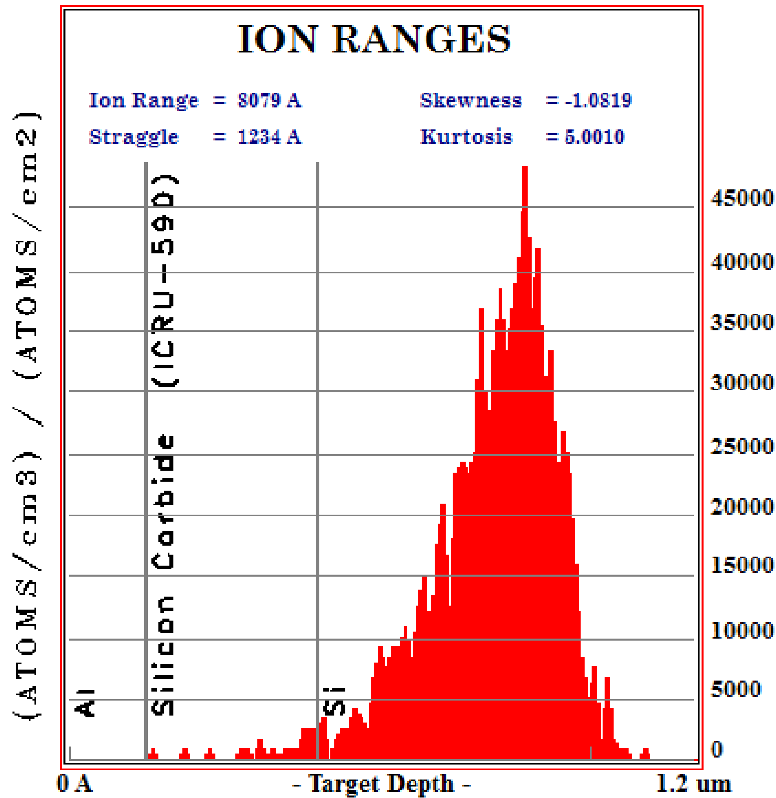

Figure 3.13 Ion Ranges for Al/SiC(328.5 nm)/Si Structure

The average range of a 1 MeV silicon ion implanted into the Al/SiC/Si structures is 0.8242 μm when the 3C-SiC thickness is 178.5 nm. The average range decreases to 0.8079 μm when the 3C-SiC thickness is 328.5 nm. The aluminum conctacts, on average decreased the ion ranges between 0.15 to 0.2 μm. Figures 3.12 and 3.13 both indicate a small number of interstitials in the silicon carbide layers. The collision event plots below provide the information needed to calculate the dpa of Al/SiC/Si structures.

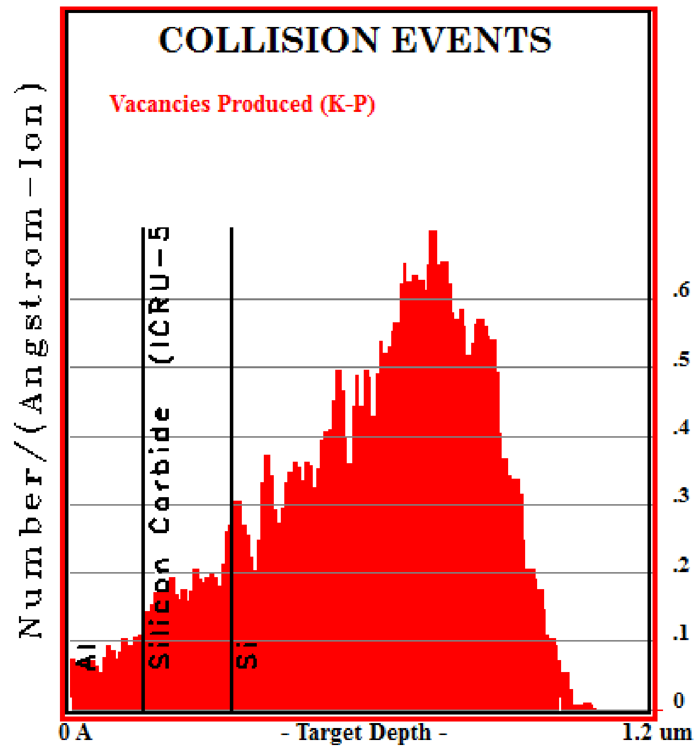

Figure 3.14: Collision Events for Al/SiC(178.5 nm)/Si Structure

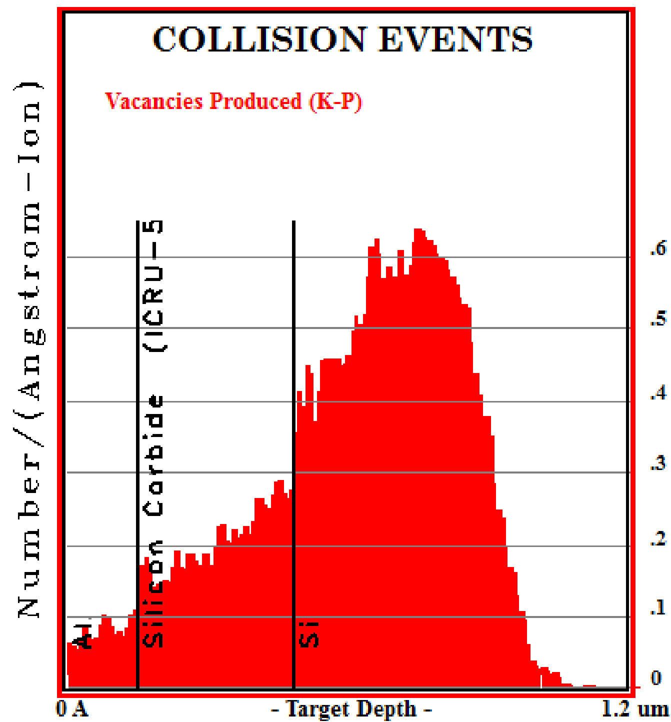

Figure 3.15: Collision Events for Al/SiC(328.5 nm)/Si Structure

TRIM analysis provides several important pieces of information including ion path, distribution, and number of vacancies produced per ion. The data obtained from the collision event plots are particularly important since the vacancies produced per ion data will be used to determine dpa (chapter 5).

Chapter 4

Characterization Methods

4.1 Keithley® 4200 SCS and Four Point Probe

There are several methods of determining the electrical characteristics of a device on a wafer. In order to perform these tests, a characterization system was purchased from Keithley® in order to measure parameters including but not limited to I-V curves and C-V curves. The tool which was utilized for electrical characterization of p-n junctions is the Keithley® 4200 Semiconductor Characterization System (SCS) which is pictured below in Figure 4.1.

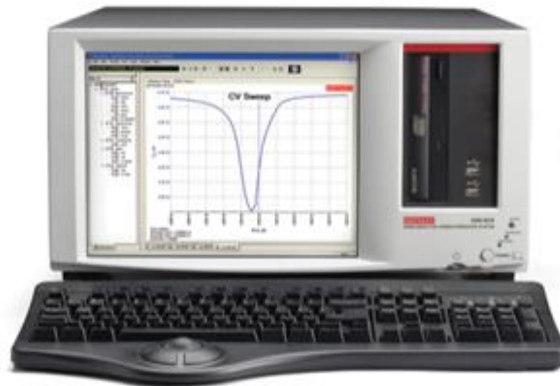

Figure 4.1: Keithley® 4200 SCS used to Characterize p-n Junctions

They Keithley® SCS purchased was configured with two preamplifiers (one preamplifier for each electrical contact) which allowed for the measurement of current-voltage parameters on scales in the femtoamphere level. The resolution of the system allows for precise measurement of electrical parameters, allowing the user to detect any shifts in electrical properties resulting from low levels of radiation damage which otherwise may not be visible from TEM imaging.

The electrical connections of the Keithley® 4200 allow the system to be connected to a probing station via coaxial cables where the electrical properties of p-n diodes are measured. Once connected to a probing station, pins were placed on the ohmic contacts on the samples which then created a circuit where resulting current values could be measured for a range of electrical potentials. The Keithley® system then recorded and stored the data in Excel tables so that the results could be later analyzed. The Keithley® 4200 SCS presents numerous benefits, not only including its precision, but in its transportability. The future goal of the investigation for measuring I-V curves on p-n junctions is to make in-situ measurements at a radiation source. Once these devices are fabricated, the Keithley® 4200 SCS can be transported to the ion beam at the University of Tennessee and real time I-V curves can be generated as the ion beam bombards the p-n junctions. This type of test will allow for real time monitoring of radiation damage in the 3C-SiC which may be applied in the future to extreme environment applications. Once this data is obtained the relation between radiation damage and electrical properties can be correlated, yielding a greater understanding of radiation effects in silicon carbide.

The configuration of the Keithley® 4200 with two current preamplifiers allows for the measurement of electrical properties on devices with two contacts. In order to measure other properties, including sheet resistivity of samples, additional preamplifiers are necessary. The measurement of sheet resistivity requires four electrical contacts. Since the addition of preamplifiers to the Keithley® 4200 SCS are expensive, and require the shipment of the system to the manufacturer, a four-point probe (pictured below) was utilized for the measurement of sheet resistivity of 3C-SiC samples.

Figure 4.2: Four-Point Probe used for Resistivity Measurements of SiC [6]

The four-point probe works by passing a range of electrical current values through two probes, while measuring the voltage on the sample with the other two probes. A common four point probe configuration with collinear contact points is illustrated below in Figure 4.3 from Schroder [41].

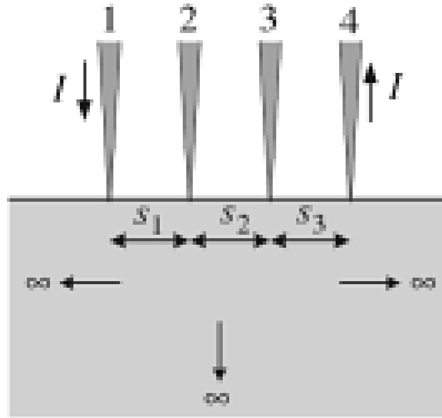

Figure 4.3: Collinear Four Point Probe Illustration

The system then computes the sheet resistance of the sample in the units of Ω/square. This value can then be converted to resistivity by multiplying the sheet resistance by the thickness of the 3C-SiC layer [29, 41]. The governing equations for the four point probe system are outlined in appendix A. Resistivity analysis will be performed on the electronically isolated 3C-SiC films illustrated in Figure 2.8. The analysis with the Keithley® 4200 SCS and four-point probe will be performed twice on samples, before and after irradiation in order to understand how electrical properties change with varying levels of radiation damage.

4.2 Resistivity Measurements

The resistivity of a material is determined by how easily current travels through the material. Since the 3C-SiC discussed in this work has been doped, it is fairly conductive with a resistivity on the order of 0.04 Ω-cm. Radiation damage creates defects in a material which therefore inhibit the flow of current through the material. The relationship between various irradiation fluences and the increase in the resistivity of bulk 3C-SiC was observed. This experiment was performed on the $SiC/SiO_2/Si$ structure outlined in Figure 2.8, cleaved into ~1 cm^2 squares. Eight samples were taken from the wafer with 178.5 nm thick 3C-SiC and another eight were taken from the wafer with 328.5 nm thick 3C-SiC. Samples were taken from wafers with two different 3C-SiC thicknesses in order to determine the effect of processing conditions on the accumulation of radiation damage. Once the samples were cleaved, preirradiation measurements were made on all 16 samples.

The preirradiation resistivities were measured using the four-point probe described in section 4.1. Each sample resistivity was measured in Ω/square then converted to Ω-cm by multiplying by the thickness of the film. Preirradiation resistivities for each of the eight 178.5 nm samples are listed below in Table 4.1. The preirradiation resistivities for the 328.5 nm are listed in Table 4.2.

Table 4.1: Preirradiation Sheet Resistance/Sample Resistivity Measurements for a 178.5 nm 3C-SiC Film

Sample	Target Fluence (ions/cm^2)	Initial Sheet Resistance (Ω/sq)	Initial Resistivity (Ω-cm)
1	$5x10^{12}$	2744	0.048980
2	$7.5x10^{12}$	2441	0.043572
3	$1x10^{13}$	2398	0.042804
4	$2.5x10^{13}$	2404	0.042911
5	$5x10^{13}$	2424	0.043268
6	$1x10^{14}$	2505	0.044714
7	$5x10^{14}$	2512	0.044839
8	$1x10^{15}$	2759	0.049248

Table 4.2: Preirradiation Sheet Resistance/Sample Resistivity Measurements for a 328.5 nm 3C-SiC Film

Sample	Target Fluence (ions/cm^2)	Initial Sheet Resistance (ohm/sq)	Initial Resistivity (ohm-cm)
9	$5x10^{12}$	1416	0.046516
10	$7.5x10^{12}$	1554	0.051049
11	$1x10^{13}$	1670	0.054860
12	$2.5x10^{13}$	1535	0.050425
13	$5x10^{13}$	1502	0.049341
14	$1x10^{14}$	1516	0.049801
15	$5x10^{14}$	1552	0.050983

*Note the final sample was not irradiated due to beam time constraints

The post irradiation analysis will be performed on the two silicon carbide thicknesses individually, but then the results will be compared. The radiation effects will be discussed in chapter 5.

4.3 Current-Voltage (I-V) Curves

The devices fabricated with 3C-SiC on bare silicon with gold and aluminum contacts are characterized by performing current-voltage (I-V) sweeps with the Keithley® 4200 SCS. The characterization was performed on each sample before it was irradiated, then redone on

each sample following the irradiations. Material parameters can vary across the surface of the entire wafer, thus the samples for irradiation were taken from a local area in the center of the wafer. The preirradiation I-V characteristics were measured for three samples and were determined to be nearly identical. The first I-V curve constructed was for the Al/SiC/Si/Au structure with 178.5 nm of 3C-SiC is displayed below in Figure 4.4.

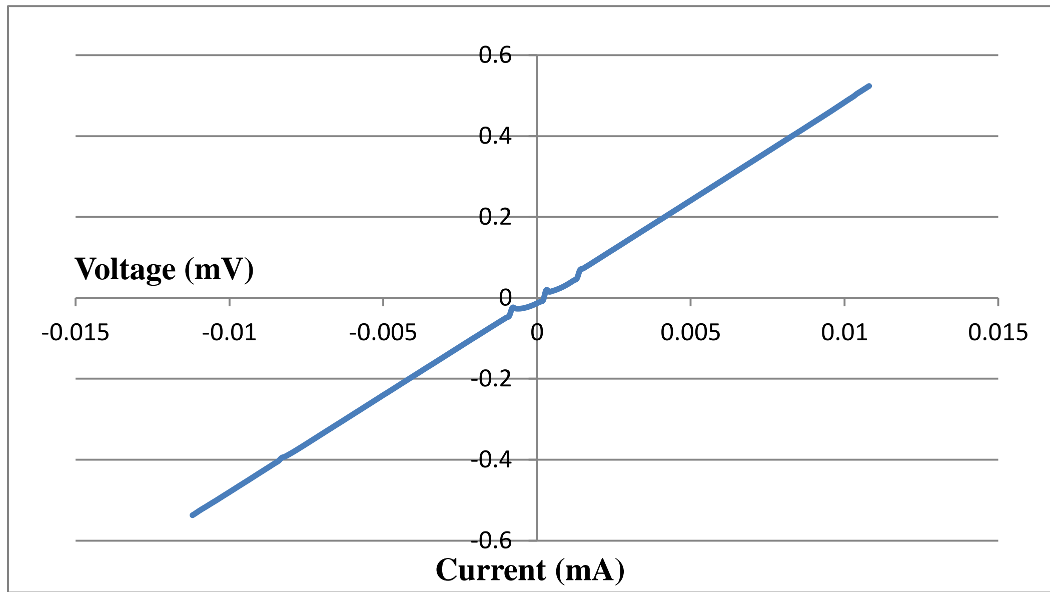

Figure 4.4: I-V Curve for Al/SiC/Si/Au Structure with 178.5 nm of 3C-SiC

The I-V curve above demonstrates a small diode characteristic at the origin, but the larger scale characteristic of the device is that of a resistor. Given the polycrystalline microstructure [19] of the 3C-SiC, ideal diode characteristics cannot be expected for this device. The defects present in the active region of the diode form traps which hinder current flow through the device, resulting in a linear characteristic. Despite the absence of a proper

diode, irradiation studies should yield changes in electrical properties similar to those of 3C-SiC sheet resistivity measurements.

I-V characteristics were also performed on the Al/SiC/Si/Au device with 328.5 nm thick 3C-SiC. The I-V characteristic curve for this device is displayed below in Figure 4.5.

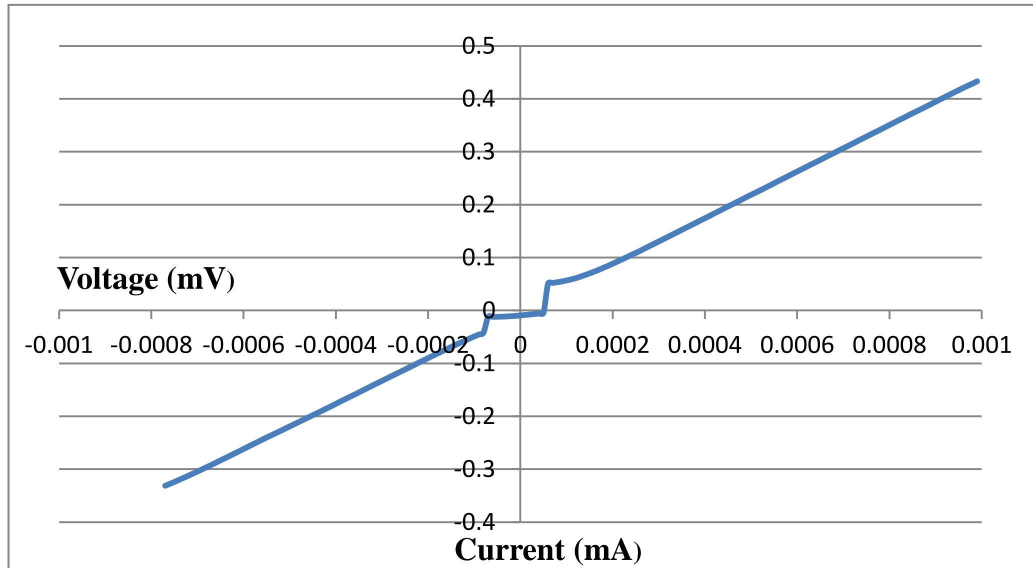

Figure 4.5: I-V Curve for Al/SiC/Si/Au Structure with 328.5 nm of 3C-SiC

Like the device fabricated with 178.5 nm of 3C-SiC, the device with a thicker silicon carbide film also displays small scale diode characteristics with larger scale resistor properties. The polycrystalline nature of 3C-SiC does not allow for the fabrication of a typical diode with which switches on at a characteristic voltage. Despite the lack of typical diode characteristics, the characteristic resistance of the device provides a parameter which can be compared pre and post irradiation. The irradiation results for these two Al/SiC/Si/Au devices are discussed in the following chapter.

Chapter 5

Results and Analysis

5.1 Resistivity vs. Fluence

The magnitude of the increase in resistivity of silicon carbide is related directly to the ion fluence used to irradiate each sample. Resistivity measurements were made on pieces of isolated 3C-SiC before irradiation and after irradiation using the same four-point probe. Initial and final values are listed below in Table 5.1.

Table 5.1 Initial and Final Resistivity Values for each 178.5 nm 3C-SiC Sample

Sample	Target Fluence (ions/cm^2)	Initial Resistivity (Ω-cm)	Final Resistivity (Ω-cm)	Increase in Resistivity (Ω-cm)
1	$5x10^{12}$	0.048980	0.053514	0.004534
2	$7.5x10^{12}$	0.043572	0.063921	0.020349
3	$1x10^{13}$	0.042804	0.079450	0.036646
4	$2.5x10^{13}$	0.042911	0.112277	0.069365
5	$5x10^{13}$	0.043268	0.150723	0.107475
6	$1x10^{14}$	0.044714	0.203490	0.158776
7	$5x10^{14}$	0.044839	8.493387	8.448548
8	$1x10^{15}$	0.049248	45.071250	45.022002

The increase in resistivity was then plot versus the irradiation ion fluence. Both axes of the plot are on log scales to allow for the clear display of all data points.

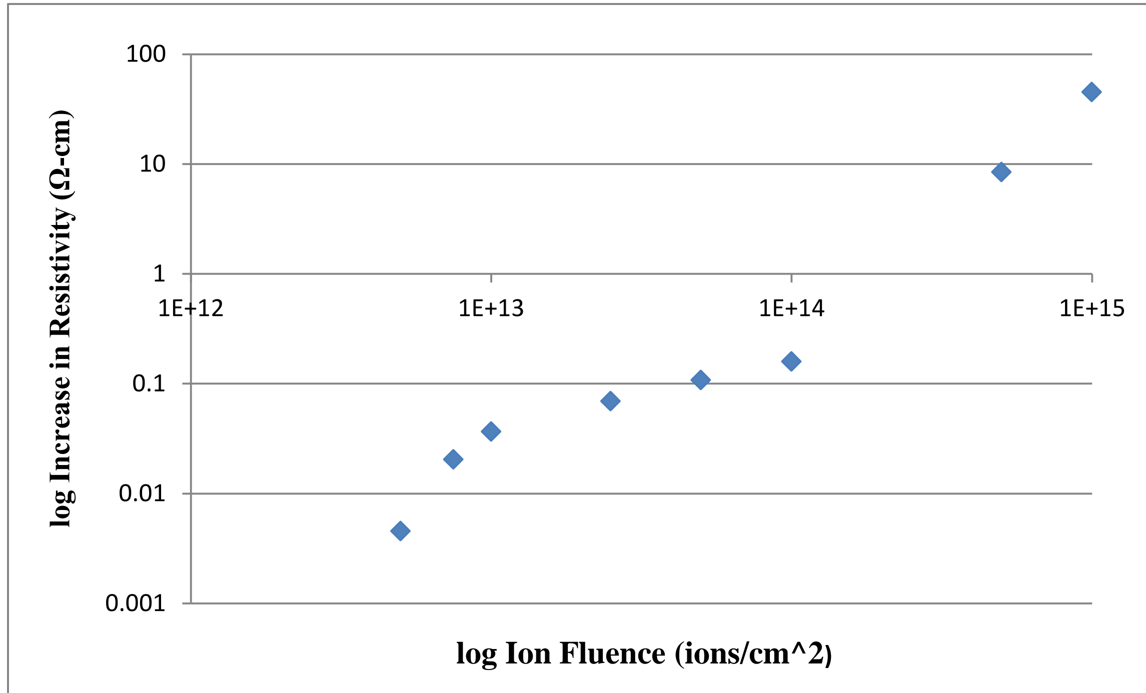

Figure 5.1: Increase in Resistivity vs. Ion Fluence for 178.5 nm 3C-SiC Films

The plot displaying the increase in resistivity as a function of ion fluence displays several trends. At low ion fluence values, the increase in resistivity is gradual, but steadily increases. At intermediate ion fluence values (up to 10^{14} ions/cm^2) the increase in resistivity appears to be reaching a maximum value at 0.158776 Ω-cm. At an ion fluence of $5\text{x}10^{14}$ ions/cm^2, the change in resistivity increases substantially. The increase occurring between $1\text{x}10^{14}$ ions/cm^2 and $5\text{x}10^{14}$ ions/cm^2 is over 50 times the previous increase value. A similar

trend is present on the samples with 328.5 nm of 3C-SiC. The increase in resistivity values for these samples is listed below in Table 5.2

Table 5.2: Initial and Final Resistivity Values for each 328.5 nm 3C-SiC Sample

Sample	Target Fluence (ions/cm^2)	Initial Resistivity (Ω-cm)	Final Resistivity (Ω-cm)	Increase in Resistivity (Ω-cm)
9	$5x10^{12}$	0.046516	0.07473375	0.028218
10	$7.5x10^{12}$	0.051049	0.1074852	0.056436
11	$1x10^{13}$	0.054860	0.1204281	0.065569
12	$2.5x10^{13}$	0.050425	0.1890846	0.138660
13	$5x10^{13}$	0.049341	0.2326437	0.183303
14	$1x10^{14}$	0.049801	0.5791455	0.529345
15	$5x10^{14}$	0.050983	51.246	51.195017

The increase in resistivity of 328.5 nm silicon carbide also undergoes a large increase between ion fluence values of $1x10^{14}$ ions/cm^2 and $5x10^{14}$ ions/cm^2. The magnitude of the change in resistivity is evident from the plot of resistivity increase versus the ion fluence in Figure 5.2. This plot, like Figure 5.1 is also on a log-log scale.

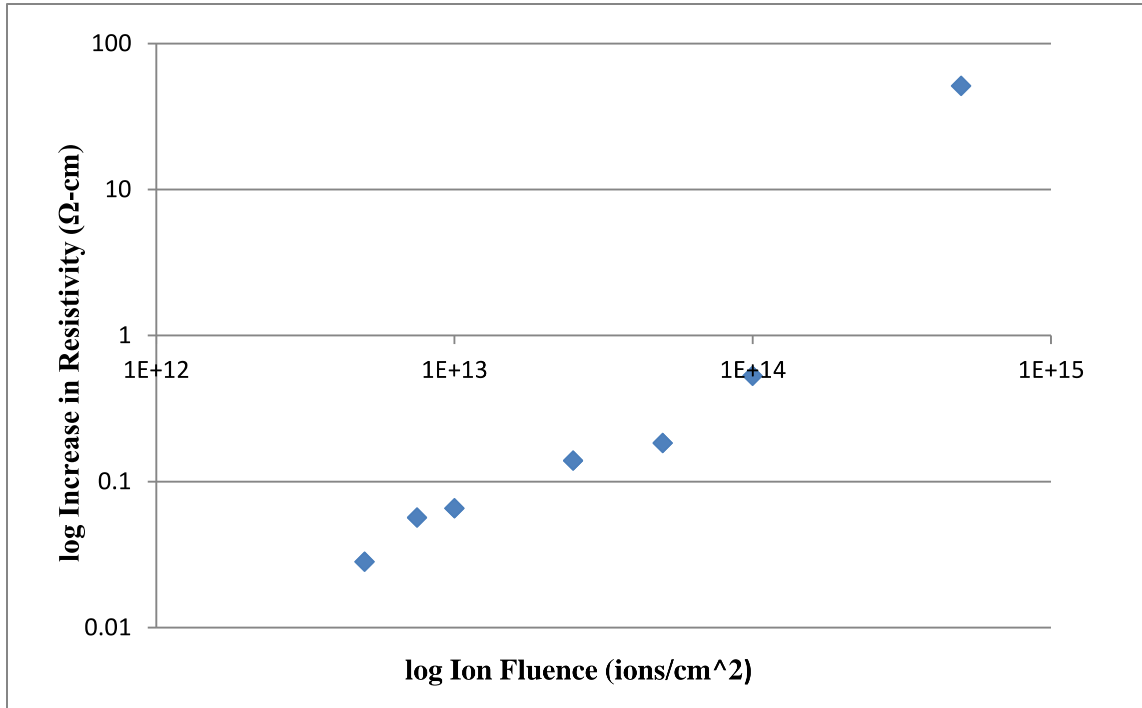

Figure 5.2: Increase in Resistivity vs. Ion Fluence for 328.5 nm 3C-SiC Films

The above plot (Figure 5.2) shares similar trends to Figure 5.1 for the 178.5 nm 3C-SiC. The data trend also begins with a gradual increase in resistivity at low ion fluence values, and then appears to be reaching a maximum value, before substantially increasing. The main difference between Figures 5.1 and 5.2 is that the transition point to large increase in resistivity values seems to be occurring at slightly lower ion fluence values. The quicker accumulation of radiation damage may be attributed to the difference in microstructure resulting from different processing conditions between the two sets of samples. These results including comparisons to the I-V curves will be discussed in the following sections of this chapter.

5.2 Resistivity vs. Fluence Analysis and Discussion

The resistivity versus ion fluence data illustrated in section 5.1 indicate that electrical characterization is an effective means of detecting low levels of radiation damage in 3C-SiC. The increase in resistivity values occurring at ion fluence values on the order of 10^{12} ions/cm^2 provide a quantifiable indication of the accumulation of point defects occurring in the 3C-SiC. In order to better understand the level of damage created by each irradiation fluence, displacements per atom (dpa) values are determined. The dpa indicates the number of target atoms in the 3C-SiC lattice displaced per silicon ion. A dpa of 1 indicates that on average, every atom in the lattice has been displaced from its original position once. The dpa values are calculated using the collision events plots in section 3.3, which were generated using TRIM software. The dpa determined by multiplying the number of vacancies N_V produced per ion occurring in the 3C-SiC by the ion fluence (ϕ), then dividing this value by the number of atoms per unit volume (V) of 3C-SiC [54]:

$$\boldsymbol{dpa = \frac{\phi * N_V}{V}} \qquad \text{Eq. 5.1}$$

The number of atoms per unit volume of 3C-SiC is 9.64x10^{22} atoms/cm^3. The number density is made with the assumption that the ratio of silicon to carbon atoms is 1:1. Using the above relation, dpa was calculated for both the 178.5 nm and 328.5 nm SiC/SiO_2/Si structures.

Table 5.3: DPA Values 178.5 nm Thick 3C-SiC Resistivity Samples

Sample	Target Fluence (ions/cm^2)	Increase in Resistivity (Ω-cm)	DPA
1	$5x10^{12}$	0.004534	0.00078
2	$7.5x10^{12}$	0.020349	0.00167
3	$1x10^{13}$	0.036646	0.00156
4	$2.5x10^{13}$	0.069365	0.00389
5	$5x10^{13}$	0.107475	0.00778
6	$1x10^{14}$	0.158776	0.016
7	$5x10^{14}$	8.448548	0.078
8	$1x10^{15}$	45.022002	0.156

Table 5.4: DPA Values 328.5 nm Thick 3C-SiC Resistivity Samples

Sample	Target Fluence (ions/cm^2)	Increase in Resistivity (Ω-cm)	DPA
9	$5x10^{12}$	0.028218	0.00093
10	$7.5x10^{12}$	0.056436	0.0014
11	$1x10^{13}$	0.065569	0.00187
12	$2.5x10^{13}$	0.138660	0.00467
13	$5x10^{13}$	0.183303	0.00934
14	$1x10^{14}$	0.529345	0.019
15	$5x10^{14}$	51.195017	0.093

Irradiations performed at ion fluence values of 10^{13} ions/cm^2 and below result in very small dpa values. For example, an ion fluence of $5x10^{12}$ ions/cm^2 causes an estimated dpa of 0.00078 for 178.5 nm 3C-SiC and of 0.00093 for 328.5 nm 3C-SiC. Using TEM imaging, it would be nearly impossible to identify damage in the crystals created at these doses. Previous TEM work has been performed on the same 3C-SiC grown by LPCVD by Zhang et al. A recent publication by Zhang et al compares TEM cross sections for unirradiated 3C-SiC films, and films irradiated at $1.2x10^{15}$ ions/cm^2 with 3 MeV Si^+ ions as seen below in Figure 5.3 below [51].

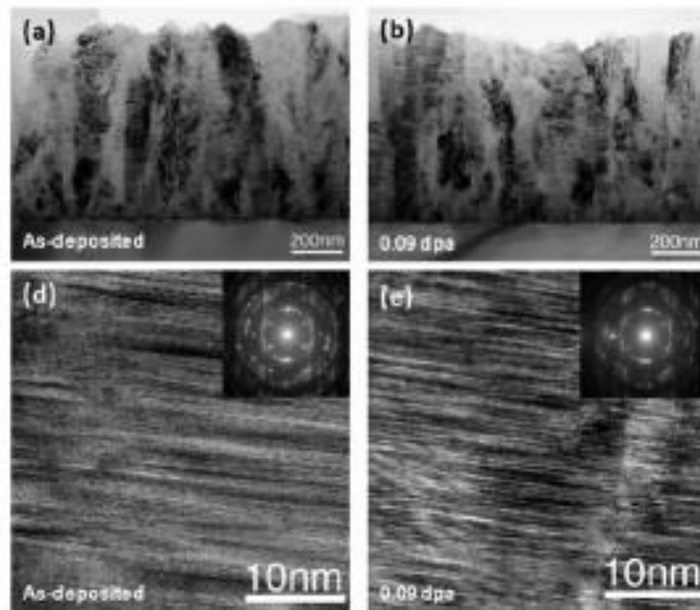

Figure 5.3: Unirradiated Films (a&d) Compared to Films Irradiated at 0.09 dpa (b&e)

The above figure indicates that at an intermediate radiation dose of 0.09 dpa, the radiation effects become visible in the TEM images and in the electron diffraction patterns of the 3C-SiC. This level of damage is caused by the clustering [51] of the accumulated vacancies. TEM images were not taken for smaller doses since there is not any significant change in the crystal structure.

The electrical characterization performed on 3C-SiC samples discussed in this chapter are a much more effective means of measuring low levels of damage than TEM imaging. A clear trend of radiation damage accumulated in the 3C-SiC as a function of dose is evident in Figures 5.1 and 5.2. An observable increase in material resistivity is evident for dpa values over two orders of magnitude smaller than the values used in the TEM images as seen Figure

5.3. The effectiveness of resistivity measurements for detection of point defect accumulation in 3C-SiC warrants future work, including simulation modeling and additional testing.

The resistivity versus ion fluence plots (Figures 5.1 and 5.2) indicate that at a fluence value of approximately ~$1x10^{14}$ ions/cm^2, an evolution of defects occurs in the crystal structure of 3C-SiC [23]. This rapid increase in resistivity can be explained with another TEM image from the study performed by Zhang et al. A second set of TEM images (Figure 5.4) compare an unirradiated 3C-SiC structure with that of one irradiated at a dpa of 0.49.

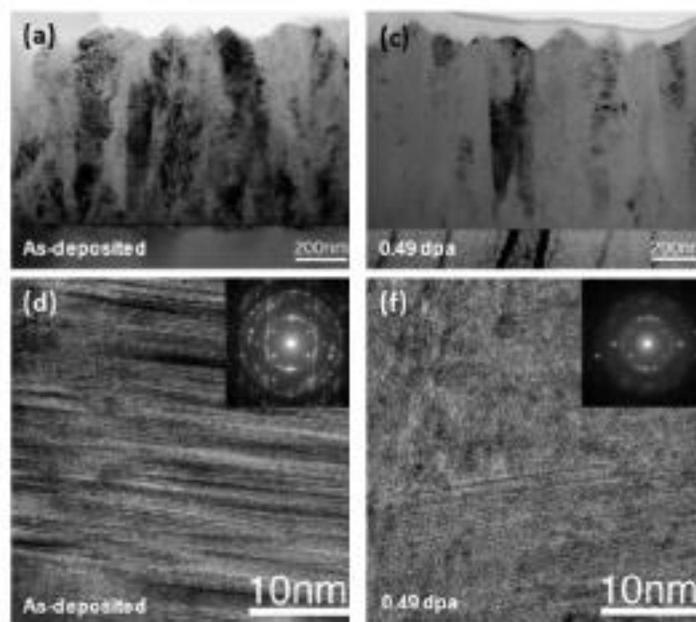

Figure 5.4: Unirradiated Films (a&d) Compared to Films Irradiated at 0.49 dpa (c&f)

Although significant damage accumulation occurs at ion fluences of $5x10^{14}$ ions/cm^2 and above, the large increase in resistivity can also be attributed to a change in contact resistance of the 3C-SiC. At larger damage levels, the quality of the film surface which comes into

contact with the four-point probe degrades. The increased contact resistance then contributes to the change in sheet resistance of the film when measured. Future work will be performed in order to distinguish the contribution of contact resistance to sheet resistance.

The accumulation of radiation damage in 3C-SiC irradiated at 0.49 dpa is much more evident than that of 3C-SiC irradiated at a dpa of 0.09. The 3C-SiC irradiated at 0.49 dpa is described by Zhang as having a “lamellar crystalline/amorphous structure”. The 3C-SiC begins to exhibit a level of amorphization, while maintaining some crystalline properties evident from the electron diffraction patterns. Full amorphization of the 3C-SiC lattice is estimated to occur at a dpa of approximately 3 by Zhang. TEM images of full 3C-SiC amorphization have not been produced since the irradiation time required to achieve this level of damage is too long. The transition of the 3C-SiC from crystalline to crystalline/amorphous may related to the transition point in the resistivity versus ion fluence curve.

The radiation tolerance of the 3C-SiC is attributed to the stacking faults in the grains of the material. These stacking faults allow for point defect migration to the grain boundaries, where they are subsequently annihilated. The steady increase in resistivity with irradiation dose can be explained by a combination of point defect accumulation and recombination at the grain boundaries [43, 51]. As defects are created, many are annihilated resulting in only a small increase in resistivity. Once the dpa is large enough, the crystal structure begins to transition into various levels of amorphization [48] since defects are created at a rate faster than which they can recombine. Additional ion fluence data points, on

the order of $1x10^{14}$ ions/cm^2 to $5x10^{14}$ ions/cm^2 may indicate the nature of crystalline to crystalline/amorphous transition.

5.3 I-V Curves

The current voltage characteristics of the Al/SiC/Si/Au structures were determined to display the characteristics of a resistor, more so than that of a p-n diode. Despite the fact that the preirradiation I-V characteristics of the devices were not typical diodes, the devices still provided a characteristic electrical response which could be compared pre and post irradiation. Six samples from two different LPCVD runs were irradiated under the conditions described in section 3.2 of this report. Three samples from two different processing conditions were irradiated at ion fluence values of $5x10^{12}$, $5x10^{13}$, and $5x10^{14}$ ions/cm^2 with 1 MeV Si^+ ions. The first set of irradiations was performed on the samples with 178.5 nm of 3C-SiC. The post irradiation I-V characteristics are plot below in Figure 5.5 along with the I-V curve of an unirradiated device.

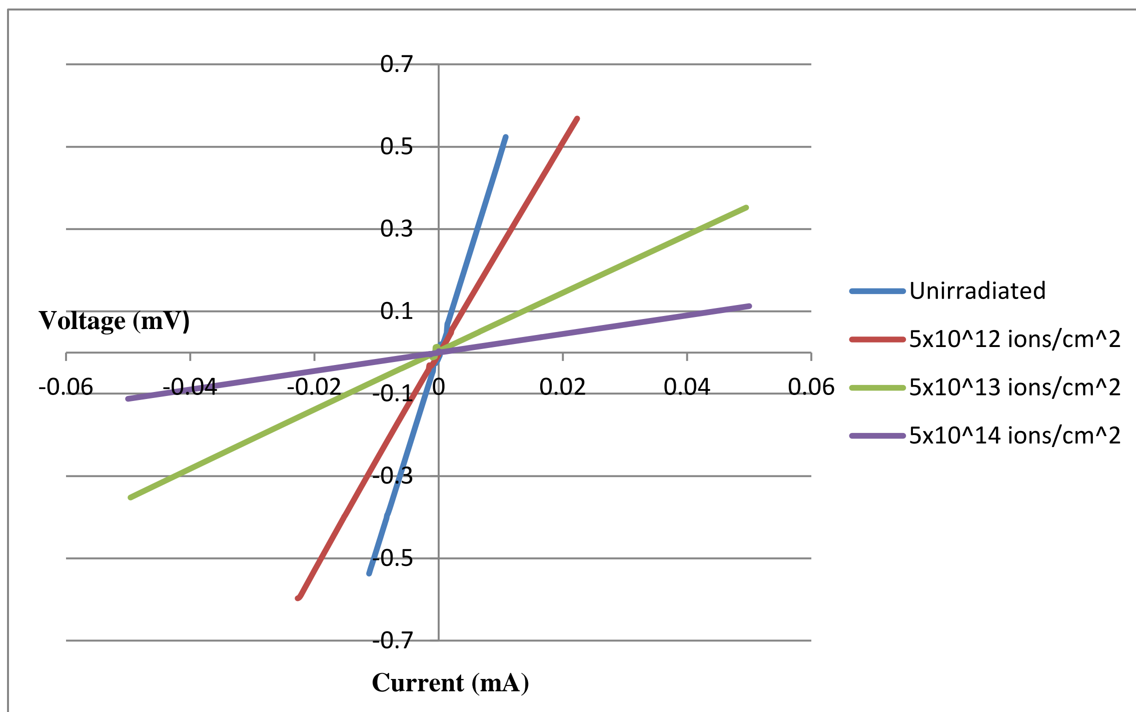

Figure 5.5: Pre and Post Irradiation I-V Curves for the Al/SiC(178.5nm)/Si/Au Device

The blue line in the above plot represents the I-V characteristics of the unirradiated device. The devices subsequently irradiated with the three ion fluence values each undergo a decrease in the slope, indicating a decrease in the conductance of the devices. The resistance is given by the inverse of the slope which increases as a function of irradiation ion fluence. A similar trend can be observed for the devices with 328.5 nm of 3C-SiC as seen in Figure 5.6 below. The conductance of the devices, indicated by the slope, also decreases as a function of the ion fluence like the I-V curves plot in Figure 5.5.

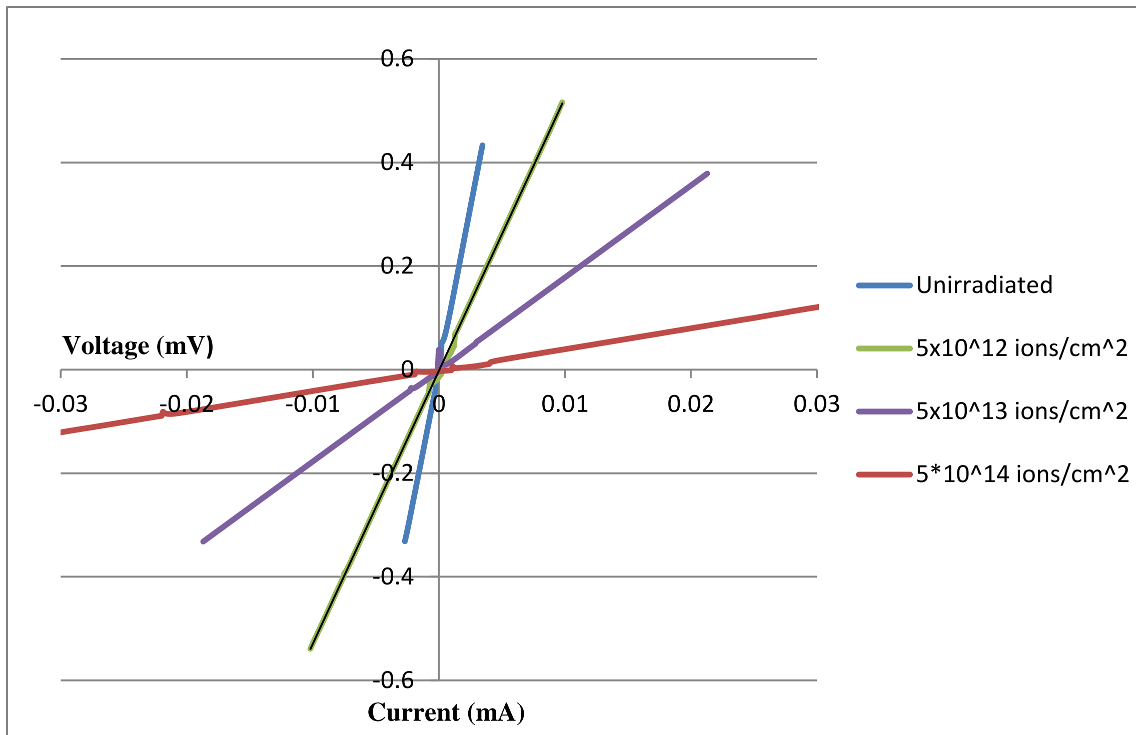

Figure 5.6: Pre and Post Irradiation I-V Curves for the Al/SiC(328.5nm)/Si/Au Device

5.4 I-V Curve Analysis and Discussion

The trend of I-V curve slope broadening as a function of ion fluence agrees with the resistivity increases observed. A similar analysis was performed on the Al/SiC/Si/Au samples. The first calculation made for these samples was dpa. The dpa values are determined using the defects created per ion plot generated from TRIM along with equation 5.1. These values are listed below in Table 5.5.

Table 5.5: DPA Values for Al/SiC/Si/Au Structures with 178.5 nm and 328.5 nm of 3C-SiC

Experiment	Target Fluence (ions/cm^2)	DPA Al/SiC(178.5nm)/Si/Au	DPA Al/SiC(328.5nm)/Si/Au
1	5x10^{12}	0.00104	0.00114
2	5x10^{13}	0.01	0.011
3	5x10^{14}	0.104	0.109

The dpa values determined above are slightly larger than the ones for comparable ion fluence in the resistivity samples. This increase is attributed to the change in ion/collision energies in the 3C-SiC layer caused by the layer of aluminum on top of it. The dpa values for the ion fluences are similar between the 178.5 nm and 328.5 nm 3C-SiC films. The slope of the I-V characteristics is what indicates the level of damage accumulation in the devices.

The accumulation of radiation damage in the Al/SiC/Si/Au devices is compared to the resistivity by determining the increase in resistance for each ion fluence. The slopes (conductance) of each I-V curve; pre and post irradiation was determined and then converted to resistance by taking the inverse of the value. The resistance values are then compared to the resistivity by comparing the increase from sample to sample. This data for 178.5 nm 3C-SiC films are listed below in Table 5.6.

Table 5.6: Increase in Resistance and Resistivity Comparison for Al/SiC/Si/Au and Electronically Isolated 3C-SiC Samples with a Film Thickness of 178.5 nm

	Conductance (S)	**Resistance (Ω)**	**Increase**	**Resistivity (Ω-cm)**	**Increase**
Unirradiated	31.2640	0.0320		0.0490	
5x10^12	22.9640	0.0435	1.3614	0.0535	1.0926
5x10^13	7.8030	0.1282	2.9430	0.1507	2.8165
5x10^14	1.2518	0.7988	6.2334	8.4934	56.3510

The calculations performed above are repeated for the Al/SiC/Si/Au and resistivity samples with a 3C-SiC film thickness of 328.5 nm.

Table 5.7: Increase in Resistance and Resistivity Comparison for Al/SiC/Si/Au and Electronically Isolated 3C-SiC Samples with a Film Thickness of 328.5 nm

	Conductance (S)	**Resistance (Ω)**	**Increase**	**Resistivity (Ω-cm)**	**Increase**
Unirradiated	125.05	0.007996801		0.046516	
5x10^12	52.67	0.01898614	2.3742168	0.074734	1.606629977
5x10^13	17.758	0.056312648	2.9659872	0.2326437	3.112956619
5x10^14	3.4619	0.288858719	5.1295531	51.246	220.276758

The increase in resistance and resistivity values for both sets of samples are of similar magnitudes for small irradiation ion fluences. Ideally, the rate of increase of the resistance and resistivity should be identical since resistance and resistivity are directly related through a geometry term. The differences in increases can be attributed to several factors. The

thicknesses of each film are an approximation, since there is a variation in deposition rate from wafer to wafer in the LPCVD furnace. The sample area also plays a role in resistance. There is a difference in sample area since the resistivity samples were slightly larger to allow for measurement with a four point probe. These geometry factors can contribute to small differences to the increase of resistance in resistivity as ion fluence is increased. Despite some inaccuracies between resistance and resistivity, the Al/SiC/Si/Au is successful at detecting the accumulation of radiation damage at low levels.

The I-V curve characterization of the devices is successful at illustrating changes in electrical properties of 3C-SiC as a function of radiation dose. Even at a low dpa dose of ~0.001, there is a quantifiable change in electrical parameters whose trends continue to change as higher radiation doses are applied. The point where the I-V curve increase in resistance rate is significantly different than the increase rate of resistivity is at large ion doses. For irradiation fluences between $5x10^{13}$ ions/cm^2 and $5x10^{14}$ ions/cm^2; the increase in resistivity was 56 and 220 times the previous value for the 178.5 nm and 328.5 nm samples respectively. For comparison, the increase in resistance for the same ion fluences is 6.23 and 5.13 times the previous value for the 178.5 nm and 328.5 nm samples respectively. This significant difference could be due to the effect of the silicon on the I-V curves. In chapter two, devices were fabricated with the goal of placing the active region of the device primarily in the silicon carbide. The location of the active region is dependent on the dopant concentration of each layer compared to the other. At large ion fluences, significant changes are made to both the 3C-SiC and the silicon on the SiC/Si interface. The large number of

defects being created in the 3C-SiC and in the interface, may have possibly changed the distribution of dopants in the materials. This change would then result in a device with a different active region and thus I-V characteristic. Despite some inconsistencies between electrical performance of the resistance and resistivity samples at high ion doses, their performance at low ion doses was successful.

The I-V characterization of Al/SiC/Si/Au devices successfully demonstrated changes in electrical properties of 3C-SiC at low ion doses. These results along with the resistivity curves indicate an accumulation of point defects which otherwise would be difficult to characterize. Electrical characterization has proved to be an effective method of determining 3C-SiC response to low levels of damage.

Chapter 6

Conclusions and Future Work

6.1 Conclusions

The 3C-SiC polytype is an important candidate material for application in future nuclear systems. Given its outstanding high temperature mechanical properties and its radiation tolerance, 3C-SiC is a candidate material for next generation nuclear TRISO fuel partial coatings and fuel cladding. The polycrystalline 3C-SiC grown via LPCVD discussed in this work has a high degree of radiation tolerance. The radiation tolerance of the material is attributed to the large number of stacking faults in the 3C-SiC which aid in the recombination of point defects resulting from damage events. The studies performed in this work served to characterize the onset and accumulation of radiation damage using the electrical properties of the silicon carbide.

The resistivity of a material is a function of the number of charge carriers, and the mobility of those charge carriers in the material. By depositing 3C-SiC on a layer of silicon dioxide, the resistivity of the thin film is isolated from that of the substrate. Subsequent radiation experiments performed on the samples indicated that the rate of accumulation of damage changed based on radiation ion fluence. At low levels of damage (10^{12} - 10^{13} ions/cm^2) resistivity gradually increases before appearing to reach a maximum value. At high levels of damage (over 10^{14} ions/cm^2) the material resistivity dramatically increases as

the microstructure becomes more damaged. A trend similar to resistivity was also observed in the current voltage characteristics of the silicon carbide.

In addition to the study of sheet resistance, p-n junctions were fabricated with 3C-SiC in order to determine the radiation effects on their I-V characteristics. In order to fabricate these devices, n-type 3C-SiC was grown on p-type silicon substrates with the active region of the device primarily in the silicon carbide. These devices had small scale diode characteristics, but the device acted mainly as a resistor given the large number of defects present in the 3C-SiC. The devices still functioned to indicate the accumulation of radiation damage as the slopes of the I-V curves broadened to indicate various damage levels in the material. These characterization methods provided a useful means of quantifying low levels of radiation damage in silicon carbide which would otherwise not be visible using techniques such as TEM imaging.

The most common application of 3C-SiC is in harsh high temperature environments. Given this application, it is important to understand the accumulation of damage in 3C-SiC. This work investigated the electrical response of 3C-SiC to radiation damage, which proved to be an effective method of quantifying various levels of damage. Continued studies will be placed on characterizing 3C-SiC and understanding the evolution of defects in the lattice.

6.2 Future Work

The work discussed in this report holds many paths for future investigation. Using similar techniques outlined in the previous chapters, it is possible to perform in-situ testing on electrical samples. With a probing system incorporated into the vacuum chamber used to house the radiation samples at UT-Knoxville, in-situ electrical measurements can be made during irradiation. The Keithley® 4200 SCS can be used to make real time measurements and store the results for analysis. This type of testing would be useful to determine the level of radiation damage in a material while it is in a high temperature, high radiation environment. This type of testing would be quicker and simpler to perform than mechanical testing.

Further investigation into the radiation tolerant properties of silicon carbide is important. The polycrystalline 3C-SiC discussed in this report has excellent radiation tolerance, but future work should be placed in analyzing the microstructure to further improve the radiation tolerance of silicon carbide. According to previous studies, the presence of a large density of stacking faults contributes to the radiation tolerance of the 3C-SiC. These defects aid in the recombination of point defects created in the material. Since microstructure is heavily dependent on processing conditions, it may be possible to engineer the stacking fault density of the material by varying these parameters [50]. If the stacking fault density is controllable, the techniques in this work may be used to determine if silicon carbide can be engineering to be more radiation tolerant.

The characterization of resistivity performed in chapters 4 and 5 indicated different regimes of damage accumulation in the 3C-SiC lattice. If the microstructure of the material was engineered to be more radiation tolerant, the transition of the curve would occur at higher ion fluences. This experiment can be performed on 3C-SiC films with varied processing conditions in order to determine if those conditions improved the radiation tolerance of the material. In addition, the effect of contact resistance on the resistivity of the 3C-SiC films will be considered. With these studies performed, recommendations for improving radiation tolerance 3C-SiC can be made.

One of the main objectives of this work is to characterize low levels of radiation damage. Ion fluence values of less than $5x10^{12}$ ions/cm^2 is difficult to obtain using the ion beam at UT-Knoxville because the irradiation time is already on the order of seconds. A future experiment which could also be performed would be the irradiation of the 3C-SiC devices with neutrons in the PULSTAR nuclear reactor at NCSU. This experiment would be helpful for understanding the accumulation of neutron damage versus ion damage. Additionally, reactor parameters such as power could be varied for irradiation experiments and the damage accumulation as a function of reactor power could be studied.

REFERECNES

[1] Chapter 10. Sputtering and Other Physical Deposition Processes." In *Tribology Series*. Vol. Volume 35, 153-178: Elsevier. http://www.sciencedirect.com/science/article/pii/S0167892299800133.

[2] Chemical Vapor Deposition. Dow Cornering Corning Corporation, 2000-2012

[3] "Materials for Nuclear Power Generation: Fuel and Cladding." University of Cambridge, http://www.doitpoms.ac.uk/tlplib/nuclear_materials/fuel.php.

[4] "SiC – SiC: Band Structure and Carrier Concentration. http://www.ioffe.rssi.ru/SVA/NSM/Semicond/SiC/bandstr.html.

[5] NCSU Nanofabrication Facility

[6] Brandt, C. D., R. C. Clarke, R. R. Siergiej, J. B. Casady, S. Sriram, A. K. Agarwal, and A. W. Morse. "Chapter 5 SiC for Applications in High-Power Electronics." In *Semiconductors and Semimetals*. Vol. Volume 52, 195-236: Elsevier.

[7] Bremner, S. 2009. *The p-n Junction ELE620 Solar Electrical Systems* The University of Delaware.

[8] Charles, C. "Shapes and Sizes of SiC." ArsAurea Gems Gems, http://www.moissaniteitalia.com/eng/caratteristiche/politipismo.htm.

[9] Chung, G. S., J. H. Ahn, and K. B. Han. 2008. "Fabrication of Poly 3C-SiC Thin Film Diodes for Extreme Environment Applications."*Industrial Electronics*: 2576-2579.

[10] Chung, Gwiy-Sang and Jeong-Hak Ahn. 2008. "Characterization of Polycrystalline 3C–SiC Thin Film Diodes for Extreme Environment Applications." *Microelectronic Engineering* 85 (8): 1772-1775.

[11] Chung, Gwiy-Sang and Chang-Min Ohn. 2008. "Ohmic Contacts to Polycrystalline 3C–SiC Films for Extreme Environment Microdevices."*Ceramics International* 34 (4): 837-840.

[12] Codreanu, C., M. Avram, E. Carbunescu, and E. Iliescu. 2000. "Comparison of 3C–SiC, 6H–SiC and 4H–SiC MESFETs Performances."*Materials Science in Semiconductor Processing* 3 (1–2): 137-142.

[13] Dmitriev, V. A. and M. G. Spencer. "Chapter 2 SiC Fabrication Technology: Growth and Doping." In *Semiconductors and Semimetals*. Vol. Volume 52, 21-75: Elsevier.

[14] Eid, J. and I. G. Galban. 2008. "3C-SiC Growth on Si Substrates Via CVD: An Introduction." *Physics of Advanced Materials Winter School*: 1-8.

[15] Fu, Xiao-An, Jeremy L. Dunning, Christian A. Zorman, and Mehran Mehregany. 2005. "Polycrystalline 3C-SiC Thin Films Deposited by Dual Precursor LPCVD for MEMS Applications." *Sensors and Actuators A: Physical* 119 (1): 169-176.

[16] Grove, A. S. B. E. Deal, E. H. Snow and C. T. Sah "Investigation of Thermally Oxidized Silicon Surfaces using Metal-Oxide-Semiconductor Structure :, Solid-State Electronics, 145 (1965)." 1965.*Microelectronics Reliability* 4 (3): 309.

[17] Hardiman, C. M. 2013. "Characterization of the Effect of Radiation Damage on the Thin-Film Stress Behavior of Nanocrystalline 3C-SiC." Master of Science, North Carolina State University.

[18] Itoh, Hisayoshi, Masahito Yoshikawa, I. Nashiyama, Shunji Misawa, Hajime Okumura, and Sadafumi Yoshida. 1990. "Radiation Induced Defects in CVD-Grown 3C-SiC." *Nuclear Science, IEEE Transactions on* 37 (6): 1732-1738.

[19] Iwata, Hisaomi, Ulf Lindefelt, Sven Öberg, and Patrick R. Briddon. 2003. "A New Type of Quantum Wells: Stacking Faults in Silicon Carbide." *Microelectronics Journal* 34 (5–8): 371-374.

[20] Jackson, K. M., J. Dunning, C. A. Zorman, M. Mehregany, and W. N. Sharpe. 2005. "Mechanical Properties of Epitaxial 3C-SiC Thin Films."*Journal of Microelectromechanical Systems* 14 (4): 664-672.

[21] Kadak, A. C. 2005. "A Future for Nuclear Energy: Pebble Bed Reactors." *Int. Critical Infrastructures* 1 (4): 330-345.

[22] Kasap, S. O. 2005. ***Principles of Electronic Materials and Devices***. 3rd ed. McGraw-Hill.

[23] Katoh, Yutai, Lance L. Snead, Izabela Szlufarska, and William J. Weber. 2012. "Radiation Effects in SiC for Nuclear Structural Applications." *Current Opinion in Solid State and Materials Science* 16 (3): 143-152.

[24] Khalil, S. et al. "Multi-scale Computational Model of Fission Product Transport in Silicon Carbide" Computational Materials Group, University of Wisconsin-Madison. 2006.

[25] Kim, Kang-San and Gwiy-Sang Chung. 2009. "Growth and Characteristics of Polycrystalline 3C–SiC Films for Extreme Environment micro/nano-Electromechanical Systems." *Sensors and Actuators A: Physical* 155 (1): 125-130.

[26] Kim, Kang-San, Ki-Bong Han, and Gwiy-Sang Chung. 2010. "Analysis of Mechanical Properties of N2 in Situ Doped Polycrystalline 3C-SiC Thin Films by Chemical Vapor Deposition using Single-Precursor Hexamethyildisilane." *Physica B: Condensed Matter* 405 (2): 513-516.

[27] Kumashiro, Y. 2000. *Electric Refractory Materials*. 1st ed. NY, NY: CRC Press.

[28] Lebedev, Alexander A., Pavel L. Abramov, Sergey P. Lebedev, Gagik A. Oganesyan, Alla S. Tregubova, and Dmitrii V. Shamshur. 2009. "Influence of the Defect Density (Twins Boundaries) on Electrical Parameters of 3C-SiC Epitaxial Films." *Physica B: Condensed Matter* 404 (23–24): 4758-4760.

[29] Li, J. C., Y. Wang, and D. C. Ba. 2012. "Characterization of Semiconductor Surface Conductivity by using Microscopic Four-Point Probe Technique." *Physics Procedia* 32 (0): 347-355.

[30] Locke, C. W., A. Severino, F. La Via, M. Reyes, J. Register, and S. E. Saddow. 2012. "Chapter 2 - SiC Films and Coatings: Amorphous, Polycrystalline, and Single Crystal Forms." In *Silicon Carbide Biotechnology*, 17-61. Oxford: Elsevier.

[31] Mattox, Donald M. 2010. "Chapter 6 - Vacuum Evaporation and Vacuum Deposition." In *Handbook of Physical Vapor Deposition (PVD) Processing (Second Edition)*, 195-235. Boston: William Andrew Publishing.

[32] Nagappa, Sharvani, Marc Zupan, and C. A. Zorman. 2008. "Mechanical Characterization of Chemical-Vapor-Deposited Polycrystalline 3C Silicon Carbide Thin Films." *Scripta Materialia* 59 (9): 995-998.

[33] Nava, F., E. Vittone, P. Vanni, G. Verzellesi, P. G. Fuochi, C. Lanzieri, and M. Glaser. 2003. "Radiation Tolerance of Epitaxial Silicon Carbide Detectors for Electrons, Protons and Gamma-Rays." *Nuclear Instruments and Methods in Physics Research Section A: Accelerators, Spectrometers, Detectors and Associated Equipment* 505 (3): 645-655.

[34] Neudeck, P. G., J. A. Powell, and L. G. Matus. 1993. "Greatly Improved 3C-SiC p-n Junction Diodes Grown by Chemical Vapor Deposition." *IEEE Electron Device Letters* 14 (3): 136-139.

[35] Noh, Sangsoo, Xiaoan Fu, Li Chen, and Mehran Mehregany. 2007. "A Study of Electrical Properties and Microstructure of Nitrogen-Doped Poly-SiC Films Deposited by LPCVD." *Sensors and Actuators A: Physical* 136 (2): 613-617.

[36] O'Connor, T. J. 2009. "Gas Reactors-A Review of the Past, and Overview of the Present and a View of the Future."Gen IV International Forum, September 2009.

[37] Petti, D. "An Overview of the DOE Advanced Gas Reactor Fuel Development and Qualificaiton Program."US Department of Energy AGR Fuel Development and Qualification Program.

[38] Petti, D. A., P. A. Demkowicz, J. T. Maki, and R. R. Hobbins. 2012. "3.07 - TRISO-Coated Particle Fuel Performance." In *Comprehensive Nuclear Materials*, edited by Editor-in-Chief: Rudy J.M. Konings, 151-213. Oxford: Elsevier.

[39] Rao, M. V. 1995. "Al and B Ion-Implantations in 6H- and 3C-SiC." *Journal of Applied Physics* 77 (6): 2479-2485.

[40] Sawa, K. 2012. "3.06 - TRISO Fuel Production." In *Comprehensive Nuclear Materials*, edited by Editor-in-Chief: Rudy J.M. Konings, 143-149. Oxford: Elsevier.

[41] Schroder, D. K. 2006. *Semiconductor Material and Device Characterization*. Hoboken, NJ: John Wiley and Sons, Inc.

[42] Sterbentz, J. W. 2007. "Low-Enriched Fuel Design Concept for the Prismatic very High Temperature Reactor Core."U.S. DOE, May 13-18, 2007.

[43] Swaminathan, N., Szlufaraka, I. and Morgan, D. "Role of Grain Size and Grain Boundaries on Irradiation Defect Production in Nanocrystalline SiC." University of Wisconsin, 2013.

[44] Tong, Lijun; Mehregany, Mehran; Matus, Lawrence G.; "Mechanical properties of 3C SiC," *Applied Physics Letters* , vol.60, no.24, pp.2992-2994, Jun 1992

[45] Verrall, R. A., M. D. Vlajic, and V. D. Krstic. 1999. "Silicon Carbide as an Inert-Matrix for a Thermal Reactor Fuel." *Journal of Nuclear Materials* 274 (1–2): 54-60.

[46] Wasa, Kiyotaka. 2012. "3 - Sputtering Systems." In *Handbook of Sputtering Technology (Second Edition)*, 77-139. Oxford: William Andrew Publishing.

[47] Weber, W. J. "Fundamental Aspects of Radiation Effects in Ceramics."University of Tennessee, Knoxville, TN.

[48] Weber, W. J., N. Yu, and L. M. Wang. 1998. "Irradiation-Induced Amorphization in β-SiC." *Journal of Nuclear Materials* 253 (1–3): 53-59.

[49] Whitmarsh, C.L. "Review of Zircaloy-2 and Zircaloy-4 Properties Relevant to Savannah Reactor Design" ORNL Union Carbide Corporation. http://www.ornl.gov/info/reports/1962/3445605716311.pdf

[50] Yun, Jungheum, Tetsuo Takahashi, Yuuki Ishida, and Hajime Okumura. 2006. "Dependence of Stacking Fault and Twin Densities on Deposition Conditions during 3C-SiC Heteroepitaxial Growth on on-Axis Si(0 0 1) Substrates." *Journal of Crystal Growth* 291 (1): 140-147.

[51] Zhang, Y. et al. 2012. "Nanoscale Engineering of Radiation Tolerant Silicon Carbide." *Physical Chemistry Chemical Physics* 14 (38): 13429-13436.

[52] Zhang, Jingchun, Carlo Carraro, Roger T. Howe, and Roya Maboudian. 2007. "Electrical, Mechanical and Metal Contact Properties of Polycrystalline 3C-SiC Films for MEMS in Harsh Environments." *Surface and Coatings Technology* 201 (22–23): 8893-8898.

[53] Zhegbroeck, B. V. "Chapter 4: P-n Junctions." University of Colorado http://ecee.colorado.edu/~bart/book/book/chapter4/ch4_3.htm

[54] Ziegler, James F., M. D. Ziegler, and J. P. Biersack. 2010. "SRIM – the Stopping and Range of Ions in Matter (2010)." *Nuclear Instruments and Methods in Physics Research Section B: Beam Interactions with Materials and Atoms* 268 (11–12): 1818-1823.

[55] Goldberg Yu., Levinshtein M.E., Rumyantsev S.L. in *Properties of Advanced SemiconductorMaterials GaN, AlN, SiC, BN, SiC, SiGe* . Eds. Levinshtein M.E., Rumyantsev S.L., Shur M.S., John Wiley & Sons, Inc., New York, 2001, 93-148

APPENDICES

Appendix A

Four Point Probe Governing Equations:

The electric field around each probe is a function of the current density J, the resistivity ρ, and the voltage V:

$$\varepsilon = J \cdot \rho = -\frac{dV}{dr} \quad \text{thus:} \quad J = \frac{I}{2 \cdot \pi \cdot r^2} \qquad \text{Eq. A.1}$$

The integral of the voltage from between an infinity point and a probe is:

$$\int_0^V 1\, dV = \frac{I \cdot \rho}{2 \cdot \pi} \cdot \int_0^r \frac{1}{r^2}\, dr \qquad \text{Eq. A.2}$$

Giving a voltage of:

$$V = \frac{I \cdot \rho}{2 \cdot \pi \cdot r} \qquad \text{Eq. A.3}$$

The distance between each probe is given by s_1, s_2, and s_3, thus the voltage at probe 2 is:

$$V_2 = \frac{I \cdot \rho}{2 \cdot \pi} \cdot \left(\frac{1}{s_1} - \frac{1}{s_2 + s_3} \right) \qquad \text{Eq. A.4}$$

The voltage between probe 2 and probe 3 is:

$$V = \frac{I \cdot \rho}{2 \cdot \pi} \cdot \left(\frac{1}{s_1} - \frac{1}{s_2 + s_3} - \frac{1}{s_1 + s_2} + \frac{1}{s_3} \right) \qquad \text{Eq. A.5}$$

Assuming all four probes are equally spaced from each other, the resistivity is:

$$\rho = \frac{2 \cdot \pi}{\left[\frac{1}{s_1} - \frac{1}{(s_1 + s_2)} - \frac{1}{(s_1 + s_2)} + \frac{1}{s_3}\right]} \cdot \frac{V}{I} = 2 \cdot \pi \cdot s \cdot \frac{V}{I} \qquad \text{Eq. A.6}$$

The resistivity can be expressed by the following equation where t is the material thickness:

$$R_s = \frac{\pi}{\ln(2)} \cdot t \cdot \frac{V}{I} = 4.523 \cdot t \cdot \frac{V}{I} \qquad \text{Eq. A.7}$$